J. Earth Syst. Sci. (2022)131 140
https://doi.org/10.1007/s12040-022-01871-8

Morphotectonic analysis of petroliferous Barmer rift basin (Rajasthan, India)

Mery Biswas[1], Mohit Kumar Puniya[2], Manash Pratim Gogoi[3], Swagato Dasgupta[4], Soumyajit Mukherjee[5,*] and Nihar Ranjan Kar[6]

[1]*Department of Geography, Presidency University, 86/1, College St, College Square, Kolkata 700 073, West Bengal, India.*
[2]*National Geotechnical Facility, Survey of India, 192/1 Kaulagarh Road, Dehradun, Uttarakhand, India.*
[3]*Department of Geology, Sibsagar College, Joysagar, Sivasagar, Assam 785 665, India.*
[4]*Department of Applied Geophysics, Indian Institute of Technology (ISM) Dhanbad, Dhanbad, India.*
[5]*Department of Earth Sciences, Indian Institute of Technology Bombay, Powai, Mumbai, Maharashtra 400 076, India.*
[6]*Centre for Earth, Ocean and Atmospheric Sciences (CEOAS), University of Hyderabad, Gachibowli, Hyderabad 500 046, India.*
**Corresponding author. e-mail: soumyajitm@gmail.com smukherjee@iitb.ac.in*

MS received 6 July 2021; revised 8 January 2022; accepted 18 January 2022

Geomorphologic studies can set important constraints on the petroleum geosciences of sedimentary basins. In the western Rajasthan area of Indian shield, constituting Barmer and other basins, rift-related sedimentation took place during Late Neoproterozoic to Cambrian Periods and during Mesozoic to Tertiary time. We analyze the Quaternary geomorphology of the Barmer basin mainly in terms of its watersheds by applying Digital Elevation Model aided by field verifications. In detail, we study aeolian landforms, drainage orientation, pattern, rejuvenation, terraces and abandoned gullies. Small streams display cross-valley anomalies. Gorge-like morphology in the eastern part of the basin near Sarnoo and knick-points in gullies near Lini/Sukri characterize the eastern boundary of the Barmer rift basin and parallel NE–SW river characterizes offset lineaments. Amongst the five delineated watersheds, watersheds-1 and 2 are recognised as the most tectonically active having lower index of active tectonics (IAT). This is also supported by the linear-scale parameters stream length gradient index (SL), sinuosity index (SI) and the long-profiles. Sub-watershed analysis using SL and SI of the watershed-1 disclose the tectonically active region within the basin. Micro-scale basin analysis has also been made applying several quantitative indicators. Watersheds-1 and 2 were found to be tectonically active. Using the normalized difference vegetation index (NDVI), the NW–SE line of vegetation across the Giral coal mine in the northern part of the basin indicates a shallow groundwater level ($\sim$7 mbgl), and can indicate presence of blind fractures.

Keywords. Tectonic geomorphology; structural geology; deformation mechanism; hydrocarbon prospecting.

Supplementary material pertaining to this article is available on the *Journal of Earth System Science* website (http://www.ias.ac.in/Journals/Journal_of_Earth_System_Science).

Published online: 07 June 2022

1. Introduction

The SW part of the Great Indian Desert is an integral part of the arid landscape including the Barmer rift basin. Widespread igneous activities, related to Late Proterozoic Malani Igneous suite, define the granitic and rhyolitic basements (Pandit *et al.* 1999; Sharma 2005). The terrain underwent different orogenic cycles, which ultimately peneplaned the landform since Proterozoic. Exposed old hills consist of several inselbergs. Sedimentation in the area started since the Late Neoproterozoic–Cambrian under continental to marine conditions (Dasgupta 1975; Kar 2011). Major rift-related sedimentation in the Barmer basin happened during Mesozoic and Tertiary (Beaumont *et al.* 2015; Dolson *et al.* 2015; Dasgupta and Mukherjee 2017).

Barmer basin is one of the major petroleum-producing rift basins in the Western Indian Rift System (WIRS), which is 200 km long, <40 km wide and ≤6 km deep (Bladon *et al.* 2015; Dolson *et al.* 2015). The basin consists of thick Jurassic to Eocene shallow marine to fluvial sedimentary sequences (Dasgupta and Mukherjee 2017). The major extension of the Barmer basin started with the separation of the Seychelles microcontinent from western India (70–62 Ma; Collier *et al.* 2008; Armitage *et al.* 2010, 2011) between Late Cretaceous through Paleogene.

We undertook a Quaternary geomorphic study of the Barmer basin dominantly based on primary and secondary field surveys applied on channel geometries (figure 1A). It involves remote sensing-based data analysis for linear aspects and fieldwork aimed at micro-scale analysis of the valley profiles along and across the channel.

The index of active tectonics (IAT of IRAT) (Mahmood and Gloaguen 2012) has been adopted to assess and class the watersheds/basins as a measure of active tectonic magnitudes (low to very high). The two main approaches in this article have been (i) watersheds delineation in the basin applying the spatial and linear-scale geomorphic indicators to identify the active watersheds; and (ii) field variation and micro-scale channel geometric analysis of the selected study points in the context of tectonics.

Rock uplift and river erosion, surface evidences (landforms, channel orientation, pattern and basin geometry) decode the tectonic activity of the watersheds in the area. We identified five watersheds out of which four are the tributaries of Sukri/Luni. Several geomorphic surfaces, e.g., terraces, elevated banks, gullies and microscale valley patterns with longitudinal valley anomalies are indications of tectonics. Previous researchers worked on stratigraphy (e.g., Dasgupta *et al.* 1975), tectonics (e.g., Bladon *et al.* 2014), sedimentation history and petroleum geology (e.g., Dolson *et al.* 2015). A geomorphologic study from this basin remained pending. Note that geomorphologic analyses have proved vital in petroleum geosciences studies (e.g., Conybeare 1976; Babu and Odeh 1994). This is because fault or basement structure can be interpreted from the drainage pattern (Sarah *et al.* 2014). Effects of such structures and neotectonics can affect surface morphology (e.g., Mazumder *et al.* 2012; Lavarini *et al.* 2016; Dasgupta and Mukherjee 2017, 2019; Dasgupta *et al.* 2022).

2. Geology and tectonics

The basement rock of the Barmer basin and adjoining areas is the Late Proterozoic Malani igneous suite/rhyolites (MIS). The basin consists of a typical rift fill shallow marine to fluvial Jurassic to Eocene sediments with major hiatus in the Late Jurassic to Early Cretaceous and in Late Cretaceous unit (review in Dasgupta and Mukherjee 2017). The Barmer basin rifted twice: (1) NW–SE extension due to E–W Gondwana separation in the Mesozoic, and (2) NE–SW extension from the K–T boundary up to the Paleocene, as India separated from the Seychelles microcontinent (review in Bladon *et al.* 2015). The main faults around the Sarnu/Sarnoo hill area at the eastern rift shoulder trends NE and ∼E, which are cut across at places by ∼NW rift faults (Dasgupta and Mukherjee 2017). The rift-related faults strike NW at the western rift shoulder in the Barmer hill area. The eastern margin of the basin is delimited by steep normal faults. On the other hand, characterize the western margin uplifted isostatically. The main rifting phase of Barmer basin, related to India–Seychelles separation, is oblique (Bonini *et al.* 1997; Dasgupta and Mukherjee 2017). Dasgupta and Mukherjee (2017) from their structural studies concluded that the fractures in the basement MIS controlled the rift structures of the Barmer basin, which is a type of structural inheritance. Pre-existing fractures guided relay

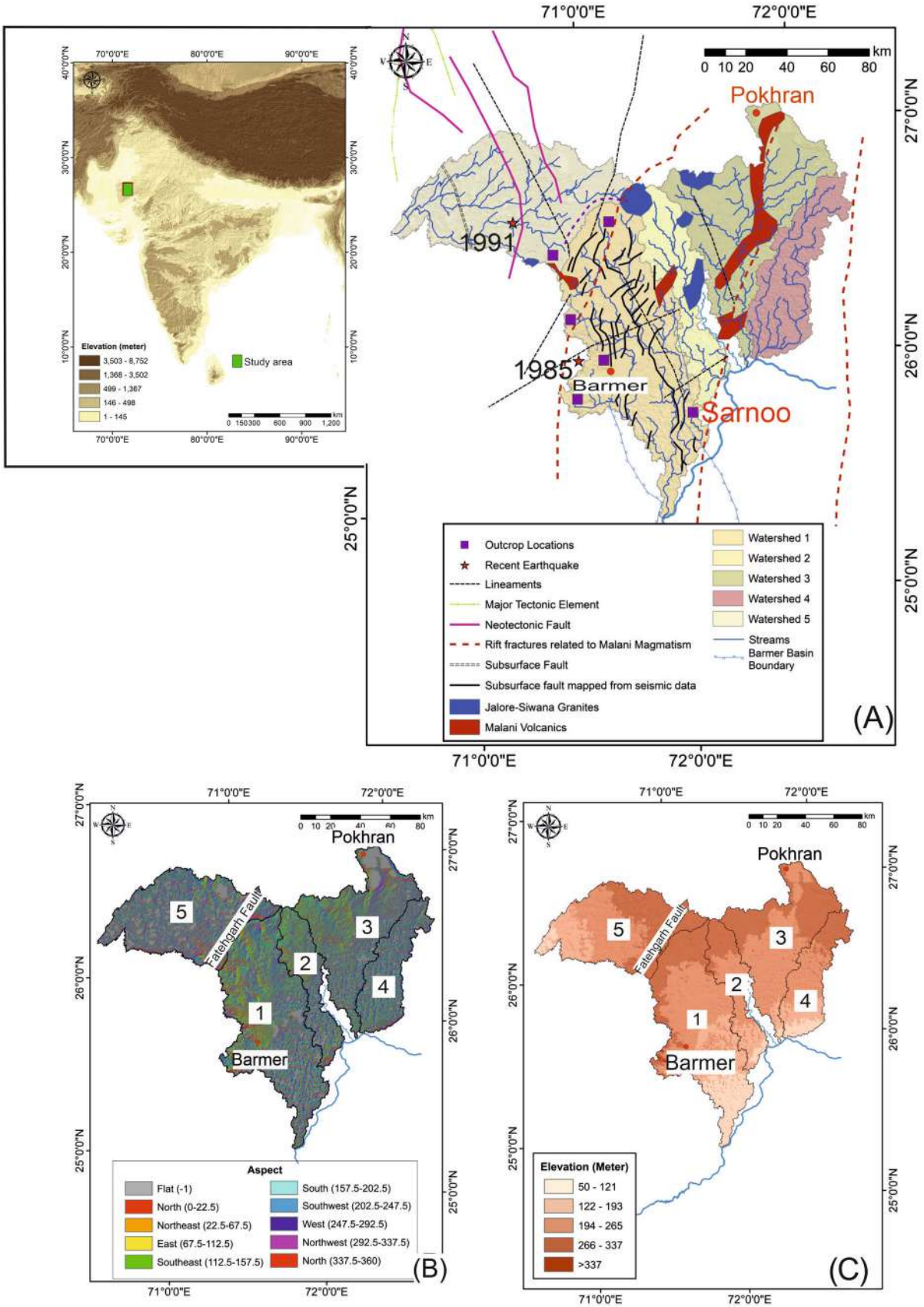

Figure 1. **(A)** Extracted and delineated from Cartosat 1 are five watersheds of Barmer basin and its adjacent areas. **(B)** Aspect slope direction map considering five watersheds at different slope directions. **(C)** Absolute relief map ranging from ~ 50 to > 337 m; higher-elevated zone is concentrated near Barmer hills area and northern arc-shaped region covering Fatehgarh Fault.

structures that govern the rift fault propagation in the basin.

3. Methodology

3.1 *Regional morphology study (before fieldwork)*

We studied relief, drainage and morphometric techniques including channel and basin geometry of the five watersheds. Exercise of the integrated morphometric techniques and geometric data analysis was based on the Digital Elevation Model (DEM), 2015 (Bhuvan Cartosat 1 of 30-m resolution). [Dataset specification: C1_DEM_16b_2005-2014_V3R1_73E24N_G43T, Theme: Terrain, Keywords: Cartosat-1, DEM, Stereo data, India, ISRO, NRSC/Use Constraints: As per NRSC Data Dissemination Policy, Purpose of creating data: Seamless DEM from IRS data, Spheroid/Datum: GCS, WGS-1984/Name of the Satellite: Cartosat-1, Sensor: PAN/2.5m, Stereo Data.]

Watersheds of river basins were delineated in the study area (figure 1A) from the extracted data from Cartosat 1 and 5. Three segments of the study have been incorporated as surface characteristics. First, this includes aspect map, elevation map, slope map, drainage analysis from drainage density, stream order and drainage pattern; and quantification of geometric indices of the basin to evaluate the index of active tectonics (IAT) (Kale *et al.* 2014). The seven indicators, *viz.*, ruggedness number (Hd), tilt angle (β), elongation ratio (Re), circularity ratio (Rc), hypsometric integral (HI), form ratio (Rf) and relief ratio (Rh) have been estimated and grouped into three classes to calculate the IAT (as per Mahmood and Gloaguen 2012).

Second, the line parameters, i.e., long profile, normalized long profile, stream length (SL) index and sinuosity index (SI) are also computed (table 1). To assess the particular point of anomalies, a break of slope along the long profile from source to mouth including SI and SL have been calculated dividing each channel into 10–11 segments. The SL has been compared with the elevation profile along the channel of each watershed to portray the anomalies. After assigning the most tectonically active watershed, linear parameters, SL and SI have been re-applied to re-evaluate the minor channels of the tectonically active watershed.

3.2 *Micro-level morphology*

We used the following dataset to demarcate the micro-basins:

- Vector file of the Indian administrative boundary (published in January 2018) collected from the India Districts ADM2 GADM ArcGIS Hub (https://hub.arcgis.com/). Using this, the administrative boundary of the study area is obtained.
- Landsat OLI 8 data of the study area from the United States Geological Survey (USGS) – Earth Explorer (https://earthexplorer.usgs.gov/) (launched February 2013, OLI 8 imagery of 2020 used for the study).
- Advanced Land Observing Satellite (ALOS) Global Digital Surface Model 'ALOS World 3D-30m (AW3D30)' from the Earth Observation Research Centre, Japan Aerospace Exploration Agency (https://www.eorc.jaxa.jp/ALOS/en/aw3d30/index.htm).
- Sentinet-2 MSI Level-2A data from Copernicus, European Space Agency (ESA), European Union made available through Google Earth Engine (https://earthengine.google.com/).
- GIS software, viz., QGIS and Global Mapper to perform DEM and raster-based analyses. Vector layers of drainage and lineaments were extracted using digitiser tools. In-built raster tools were used to perform profile analyses, ridge (lineament mapping), drainage analyses and hypsometric curve preparation.
- Spreadsheet software to perform statistical calculations, e.g., linear, exponential, logarithmic and power regression.
- The following morphometric parameters are used for fluvio-morphometric studies:

(a) Drainage basin asymmetry (AF) (Hare and Gardner 1985; Cox 1994; Keller and Pinter 2002):

$$AF = (Ar/At) \times 100, \tag{1}$$

where Ar is the basin area on the right and At is the total basin area.

(b) Valley floor width to height ratio (V_{fwh}) (Bull and McFadden 1977; Bull 1978):

$$V_{fwh} = \frac{2\,V_{fw}}{[(E_{ld} - E_{rd}) + (E_{rd} - E_{sc})]}, \tag{2}$$

where V_{fw} is the width of the valley floor, E_{ld} and E_{rd} are the elevations of the divide on the left and right sides of the valley, respectively. E_{sc} is the average elevation of the valley.

Table 1. *Detailed methodology for characterizing relief, drainage and channel morphometry.*

Sl. no.	Indices		Reference
		Relief characterizes	
1	Relief map	Extracted from DEM in Arc GIS10.3	NA
2	Aspect Map	Extracted from DEM in Arc GIS10.3	NA
3	Slope map	Extracted from DEM in Arc GIS10.3	
		Drainage analysis	
1	Drainage density	$D_d = L_{u/A}$ (extracted from DEM in Arc GIS10.3) L_u = total stream length, A = total area	Horton (1945), Singh *et al.* (2015)
2	Stream order	Hierarchic order	Strahler (1952)
3	Drainage pattern	Extracted from drainage map .	Morisawa (1985)
Basin scale			
		Geometric and morphometric parameters	
1	Ruggedness number	$Rn = R \times Dd$ (where R = basin relief, Dd = drainage density of the basin)	Schumm (1956)
2	Tilt angle	$\beta = \arccos[\sqrt{\{(ba)2 \sin 2\alpha + \cos 2\alpha\}}]$ (where b = minimum half-length of the basin, a = maximum half-length of basin, α = original depositional slope of basin)	Pareta and Pareta (2011)
3	Elongation ratio	$Re = 1.128\sqrt{A} \times Lb$ (where Lb = length of the basin, A = area of the river basin)	Schumm (1956)
4	Circularity ratio	$Rc = 4\pi A/P^2$ (where A = area of the basin, P = perimeter of the basin) Circular (0.9–0.10), oval (0.8–0.9), less elongated (0.7–0.8), elongated (0.5–0.7), and more elongated (< 0.5). • 0.9–1.0 Circular 0.8–0.9 Oval 0.7–0.8 Less elongated < 0.7 Elongated	Horton (1945)
5	Hypsometric integral (HI)	$HI = \frac{(H_{mean} - H_{min})}{(H_{max} - H_{min})}$ (where H_{mean} = mean elevation, H_{min} = minimum elevation, H_{max} = maximum elevation)	Strahler (1952)
6	Form factor	$Rf = A/Lb^2$ (where A = area of the basin, Lb = length of the basin)	Horton (1945)
7	Refief ratio	$Rh = \frac{R}{Lb}$ (where R = basin relief, Lb = length of the basin)	Schumm (1956)
Linear scale			
8	Normalize long profile	The linear function $y = ax + b$ The logarithmic function $y = a \ln x + b$ (where y is the elevation (H/H_0; H = elevation of each point, H_0 = elevation of the source), x is the length of the river (L/L_0; L = distance of the point from the source, L_0 = total length of the stream), a and b are the coefficients derived independently from each profile. The R^2 value determines the best fit. The curve with highest R^2 value is the best-fit curve (extracted from SRTM 30m DEM and formulated using Arc GIS 10.4 and TNT mips 2014 platform))	e.g., Paul and Biswas (2019); Kale *et al.* (2014); Lee and Tsai (2009)
9	Concavity index (Θ)	$\text{Ceh} = \frac{1}{S_2 - S_1}\Delta E$ (where S_1 is the channel slope prior to disturbance, S_2 is the channel slope after disturbance (e.g., due to a change in incision rate E) and ΔE is the difference between the incision rate before and after disturbance)	e.g., Whipple *et al.* (2007); Wobus *et al.* (2006)

Table 1. *(Continued.)*

Sl. no.	Indices		Reference
10	Stream gradient index (SL)	$SL = \frac{f}{\ln D_2 - \ln D_1}$ (where f = fall in elevation ($e_2 - e_1$), ln = natural logarithm of the cumulative distance, *higher SL value indicated tectonic control over stream)	Hack (1957)
11	Sinuosity index (SI)	$\text{SI} = \frac{\text{Channel length}}{\text{Valley length}}$ Straight channel values <1.05, straight to sinuous values between >1.05 and <1.50, Meandering channel indicates >1.50 mouth.	Biswas and Dhara (2019); Brice (1964); Schumm and Khan (1972)

(c) Sinuosity index (SI) (Mueller 1968; Haggett and Chorley 1969):

$$SI = \frac{CL}{VL}. \tag{3}$$

Here CL is the length of the channel segment and VL is the valley length.

(d) Hypsometric curve analyses (Strahler 1952) by using percentage method with two ratios, *viz.*, (h/H) and (a/A). Here a is the area at a given contour, A is the total area, h is the elevation of that contour above the lowest point in the basin, and H is the relief of the basin.

(e) Transverse topographic symmetry factor (T) (Cox 1994):

$$T = Da/Dd. \tag{4}$$

Here Da is the distance between the basin midline to an active meander belt midline, and Dd is the distance between the midline and basin divide.

(f) Regression analyses of the stream longitudinal profiles:

$$\text{(i) } \textit{Linear regression}\text{: } y = mx + b. \tag{5}$$

$$\text{(ii) } \textit{Exponential regression}\text{: } y = ae^{bx}. \tag{6}$$

3.3 *Field verification*

To conduct micro-level analysis, eight valley sections were considered to specify the minor-scale anomalies. We have covered (i) the northern Fatehgarh Fault area, (ii) the eastern rift shoulder part of the Barmer basin near Sukri/Luni river, and (iii) the location Gangli (25°41′1.21″N/71°56′31.60″E). At the eastern boundary of Barmer basin in Sarnoo, four individual spots – Sarnoo-I to IV were covered for the field verification. In the western part, field study has been conducted near Jasai village area and near the Kiradu temple around Sihani.

During fieldwork in the first quarter of 2021, elongated alignments and patches of natural vegetation and agricultural fields in this rocky desert region were observed at few places, which are devoid of any canal irrigation system. Normalized difference vegetation index (NDVI) (Ozyavuz *et al.* 2015) analysis has been used after fieldwork, which is based on remote sensing application using Landsat 8 Operational Land Manager datasets following the band equation:

$$\text{NDVI} = \frac{\text{NIR} - \text{Red}}{\text{NIR} + \text{Red}}. \tag{7}$$

It has been compared with the existing fault lines and the groundwater level in monsoon, August 2019 and post-monsoon, January 2020 (Central Ground Water Board Department of Water Resources, River Development and Ganga Rejuvenation Ministry of Jal Shakti Ground Water Year Book Rajasthan 2019–2020, Western Region, Jaipur).

4. Results and discussions

4.1 *Regional analysis of morphology based on pre-field study*

The quantitative geomorphologic analysis of the five delineated watersheds reveals the characteristics of morphotectonic parameters (Altaf *et al.* 2013). Watersheds that originated in recent times activate during monsoon. These watersheds had originated from hilly scarps of sandstone (north) and granite hills flowing over sandy pediment (Moharana *et al.* 2013), and aggraded alluvial plains since the Late Cretaceous (Singh 1977).

The major phases of the present-day arid landscape and drainage development started from the Early Holocene (Kar 1987, 1990). The main humid phase existed in Pre-Holocene. It terminated ∼10,000 years B.P. when most of the dunes (Singh 1977; Chatterje *et al.* 2013) and arid plains

developed. During 10,000 to 3800 years B.P., the climate again became humid whereas it was less humid between 9500 and 5000 years B.P. (Singh *et al.* 1971). Therefore, the present watershed geomorphology gives ample scope to study the active tectonics based on geometric indicators.

4.2 *Relief characteristics*

The relief characteristics of the Barmer rift basin are defined by isolated hills composed of granite and rhyolite near the Barmer town, towards WSW part near Jasai, further west near Kiradu temple area, etc. In the eastern rift shoulder area near Gangli and Sarnoo, isolated granite exposers and Cretaceous outcrops of Sarnoo hills exist. Towards the north, the elevated elongated Fatehgarh fault area extends W–E. In the NE part, a dome-shaped granitic exposer with a convex summit with concave basal slope is noted. The slope aspect delineates the erosion and slope sequences over the five-watershed area (figure 1B). Slopes are towards N–NE, E, SE, S–SW, W and NW. In the upper part of watershed-4 near Pokhran, it is a flat topography. Supplementary figure S1 depicts the isolated hills covering the higher slope area followed by huge elongated parabolic, coalesced parabolic dunes, and barchans. Slope ranging from 0 to 4° covers ∼45% of the watershed area. Along with the aspect and slope, elevation of the area ranges 50–350 m above asl. The easternmost pocket of watershed-5 has a higher elevation. It decreases towards the south (in watersheds 1–4) and west (part of watershed-5) ranging from 50 to 265 m above asl (figure 1C).

4.3 *Drainage analysis*

Dynamic graded river channels of the five watersheds derived from the hilly patches of the Barmer hill area are characterized mostly by rill and gully erosion. These rain-fed rivers with their tributaries are reframed by tectonics and sediment aggradation process with varying initiated flows. They are accompanied by coarser grains (>432 mm) clastic depositions in the top-layer of the dry channel and headward erosion extends till the hills, known as Inselbergs.

In figure 2(A), the five red points identify the photographic evidence of channel characteristics. The drainage orientation determines the stream order and its relation with the existing terrain. Watershed-1 is the only fifth-order stream as it flows over the piedmont plains of the Barmer basin. It is originated from the hilly scarp of the upper section near the Fatehgarh fault. With a break of slope (∼0.8 m) towards south, huge aggradation produced convex shape in its long profile. The channel is further followed by joining a number of streams from both eastern and western sides

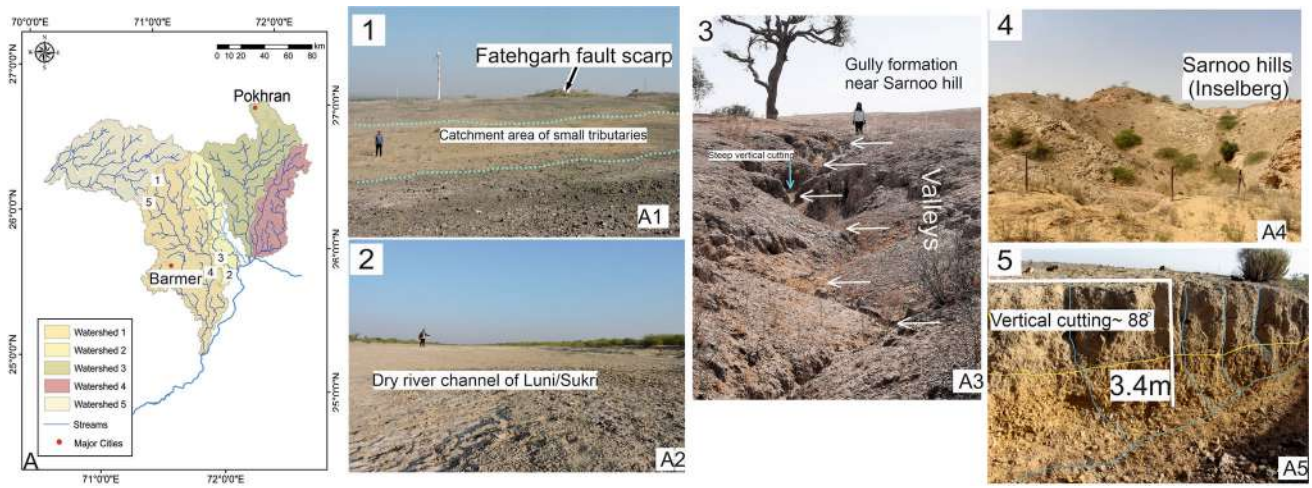

Figure 2. **(A)** Drainage map of the considered study area with distinct watersheds and images from A1 to A5 differently representing the stream characteristics of 5 points (red colour). **(A1)** Point 1 is a part of Fatehgarh Fault area. A small catchment of a tributary of watershed-1 identified towards south where S Mukherjee is facing from the Fatehgarh fault scarp (backside). **(A2)** A dry river channel of river Luni/Sukri where fine salt grains are visible. M Biswas facing towards upstream, i.e., NNE. Rocky right side bank is also prominent. **(A3)** Extensive gully formation near Sarnoo hill area with steep vertical cutting and gorge formation in the middle part of the gully. **(A4)** Elevated Sarnoo hill in point 4 forming a circular-shaped catchment and the hilly patch. **(A5)** Point 5 near Fatehgarh west part from the National Highway where deep vertical cutting of gully channel of ∼88° with two distinct weathered layers and micro-channels join at the right angle.

forming various drainage patterns. This area consists of tertiary sediments associated with subvertical volcanic ash beds underlain by granite and rhyolite. The western branches of the channel flows over several fault lines. Numerous first-order streams have originated from the hilly tracts of Jasai and Danta (Supplementary figure S2). Watershed-2 consists of third-order, and watersheds 3 and 5 are characterized by fourth-order streams. They represent a homogeneous rock basement.

Rock structure, slope and erodibility of the Barmer area have been determined by the drainage pattern and density in terms of spatial streamlines per km^2. In Supplementary figure S3(A), the drainage density map displays the drainage line accumulation towards the downstream where we spot streams with maximum stream order. Geologic structures and tectonics govern the channel network (Supplementary figure S3B).

A drainage network formed on a stable, homogeneous landscape develops a dendritic drainage pattern. It has developed in the upper catchment of watersheds 1 and 2. It resembles the spreading branches of a tree (Howard 1967) where all lines join the mainstream at different angles (Zernitz 1932). Here rocks, predominantly sandstones, are uniform and provide (nearly) the same resistance to erosion (Ansan and Mangold 2006).

Regularly-spaced right-angle joining of channels with its next order stream forming rectangular–angulate drainage pattern was identified distinctly from watersheds 1, 3 and 5 (Supplementary figure S3A). The area is tectonically active and is typically controlled by joints and faults at or near right angles. In watershed-1, NNW–SSE-aligned fault lines and SW–NE lineaments have framed the streamlines as rectangular–angulate drainage.

In watershed-3, the green-marked sub-parallel pattern (Supplementary figure S3B) represents steep slopes. Here the bedrock or landforms trend parallel to the regional slope and tributaries flow sub-parallel to each other (e.g., Twidale 2004). Contorted drainage pattern develops uniquely as hooks and bends (Howard 1967) in tributaries that join the mainstream. Contorted drainage pattern is observed in watersheds-1 and 5. It represents complex geologic history (e.g., Drummond and Erkeling 2014). Dykes and faults are documented in watershed-1 (west of Barmer town, towards Kiradu temple), north of Jasai railway station, and near Gangli (east of the Sarnoo area).

5. Geometric and morphometric parameters

To formulate the index of active tectonics (IAT), indices such as ruggedness number (Rh), tilt angle (β), elongation ratio (Re), circularity ratio (Rc), hypsometric integral (HI), form factor (Rf) and relief ratio (Rh) have been calculated for each watershed. Three classes 1, 2 and 3 have been defined to characterize the different value ranges of the morphometric parameters (Supplementary figure S4A–G).

Rh denotes the ratio between basin relief and drainage density. It also implies that the area with a higher ruggedness value is less susceptible to erosion. Watersheds-1 and 2 come under class 1 (Rh = 40.2–52.0). Watersheds 4 and 5 (Rh = 30.1–40.1) come under class 2, and lower in watershed-3 (Rh = 21.0–30.0).

Tilt angle (β) ranges from 1.97° to 1.20° in the three classes found from five watersheds. β values for class 1 includes watershed 1 and 5 ranging 1.72°–0.97°. It is followed by watershed-2 under class 2 ranging from 1.46° to 1.71° as moderate. The two other watersheds, 3 and 4, represent the low tilt ranging from 1.20° to 1.45°. Watersheds-1 and 2 are highly tilted and belong to Class-1. It is obvious, considering the maximum concentration of fault lines, lineaments, sub-surface fractures and NNE aligned rift fractures related to the Malani magmatism as available from the published literature (Dasgupta and Mukherjee 2017). This area is accompanied by several tectonic events from the Precambrian (Roy and Jokhar 2002) to the Quaternary with several intermediate volcanic episodes (Storey *et al.* 1995; Sharma 2005; Bladon *et al.* 2015).

Elongation ratio (Re) is the ratio between the diameters of a circle of the same area as the basin to the maximum basin length, and it varies from 0 to 1. Watershed-2 is less elevated with a gentle slope where the elevated patches are restricted in the northern and southernmost parts. The higher values of class 3 (Re = 0.68–0.61) including watersheds 3 and 5 are associated with high relief and steep ground slant (e.g., Prakash *et al.* 2017). Watersheds 1 and 4 have moderate Re = 0.53–0.61. This indicates that these basins are less elongated than watershed 2. Though watersheds 1–5 are overall elongated ($Re < 0.7$), we have categorized them under three classes. The most elongated watershed-2 (Re = 0.45–0.52) tends to become more circular in respect of the termination of uplift (Bull and McFadden 1977; Singh 2015) in the tectonically active area.

Calculated Parameters

Watersheds	Circularity Ratio(Rc)	Elongation Ratio (Re)	Form Factor (Rf)	HI	Relief Ratio	Ruggedness number	Tilt angle
Watershed 1	0.14	0.56	0.24	0.61	2.37	47.19	1.94
Watershed 2	0.12	0.45	0.16	0.5	2.1	48.3	1.63
Watershed 3	0.14	0.63	0.31	0.43	1.88	28.21	1.27
Watershed 4	0.16	0.58	0.27	0.4	1.95	30.6	1.25
Watershed 5	0.2	0.66	0.35	0.45	1.99	31.64	1.8

Classifications fo the parameters

Classes	Circularity Ratio(Rc)	Elongation Ratio (Re)	Form Factor (Rf)	HI	Relief Ratio	Ruggedness number	Tilt angle
Class 1	0.12-0.14	0.45-0.52	0.15-0.21	0.56- 0.63	2.22- 2.47	40.2-52.0	1.72-1.97
Class 2	0.15-0.17	0.53-0.60	0.22-0.28	0.48-0.55	1.96-2.21	30.1-40.1	1.46-1.71
Class 3	0.18-0.20	0.61-0.68	0.29-0.35	0.40-0.47	1.70-1.95	21.0-30.0	1.20-1.45

(A)

IAT Ranking

Watersheds	Circularity Ratio(Rc)	Elongation Ratio (Re)	Form Factor (Rf)	HI	Relief Ratio	Ruggedness number	Tilt angle	IAT
Watershed 1	1	2	2	1	1	1	1	1.29
Watershed 2	1	1	1	2	2	1	2	1.43
Watershed 3	1	3	3	3	3	3	3	2.71
Watershed 4	2	2	2	3	3	2	3	2.43
Watershed 5	3	3	3	3	2	2	1	2.43

(B)

IAT Class	Range	Magnitude
Class 1	1.28-1.88	High
Class 2	1.89-2.49	Moderate
Class3	2.50-3.10	Low

(C)

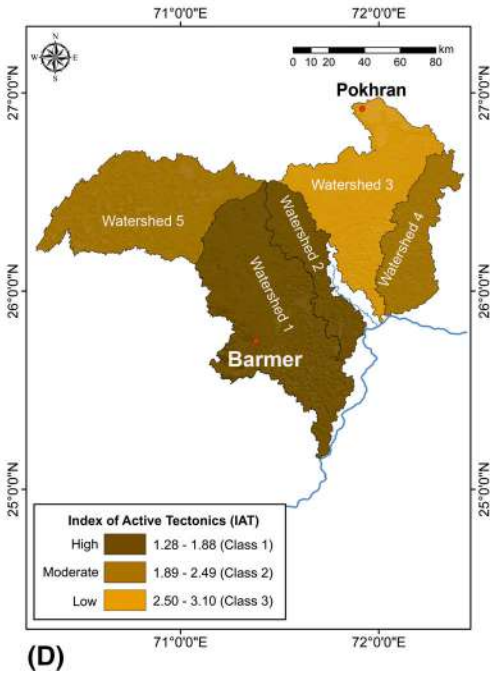

(D)

Figure 3. Calculation of parameters for IAT analysis and classification as per the obtained classes.

Circularity ratio (*Rc*) is the ratio measured from the basin area with the basin perimeter. In the Barmer basin, it ranges between 0.20 and 0.12 under three classes. The lowermost range from 0.12 to 0.14 covers watersheds-1, 2 and 3, which signify the youth stage. The higher range 0.18–0.20 displays a mature stage (watershed-5). For watershed-4, it is moderate (0.15–0.17) and under Class-2. Watersheds under Class-1 have experienced more tectonic movements that reframed the channel aggradation/degradation sequences with lateral and vertical valley incision.

Hypsometric integral (HI) can indicate tectonic activity. High Hi values indicate recent landforms resulting from active tectonics (Hamdouni *et al.* 2008). Hi from 0.56 to 0.63 indicate a lower erosion rate in the upland hilly area of watershed-1. Whereas, watershed-2 under Class-2 ranges from 0.48 to 0.55, and watersheds-3, 4 and 5 under Class-3 with Hi range from 0.40 to 0.47. It is suggested that less eroded basins are under the young stage since active tectonics make the landscape rugged (Hamdouni *et al.* 2008). Hilly terrain in watershed-1 is consists of Precambrian Malani Igneous Suite of granite-rhyolite and pre-rift Mesozoic sediments (Sisodia and Singh 2000; Torsvik *et al.* 2005; Compton 2009), which are more resistant to erosion. This watershed is also marked by a number of lineaments, fault lines and fracture lines that exhibit several tectonic events along with volcanic pyroclastic and basaltic lavas of the Raageshwari Volcanic Formation (Compton 2009).

The form factor (*Rf*) presents the ratio between the basin area and its length. Its magnitude towards 0 and 1 indicate tectonic activeness and inactiveness, respectively (Wołosiewicz 2018). We have derived three classes of Rf values ranging from 0.15 to 0.21 as class-1, 0.22–0.28 as class-2, and 0.29–0.35 as class-3. According to the classes, watersheds 1 and 4 belong to class-2, and watershed-2 in class 1. Watersheds 3 and 5 under class-3 are less active as their calculated Rf values range between 0.29 and 0.35.

Relief ratio (*Rh*) is a measure of the overall steepness of a watershed. It indicates intensity of incision on the terrain slope. *Rh* normally bears a negative correlation with drainage area and size. Higher values of Rh indicate more incision of the channels due to steep slopes or alteration of slope segments along the basin flow path. In the present study, watershed-1 under class-1 with Rh = 2.22–2.47 is more susceptible to erosion than watersheds-2 and 5 (Rh = 1.96–2.21). Whereas, watersheds-3 and 4 with Rh =1.70–1.95 are under less intense erosion.

For better assessment of the tectonic status of the region (Ziyad 2014), all the parameters have been assembled in terms of index of active tectonics (IAT) or index of relative tectonics (IRAT)

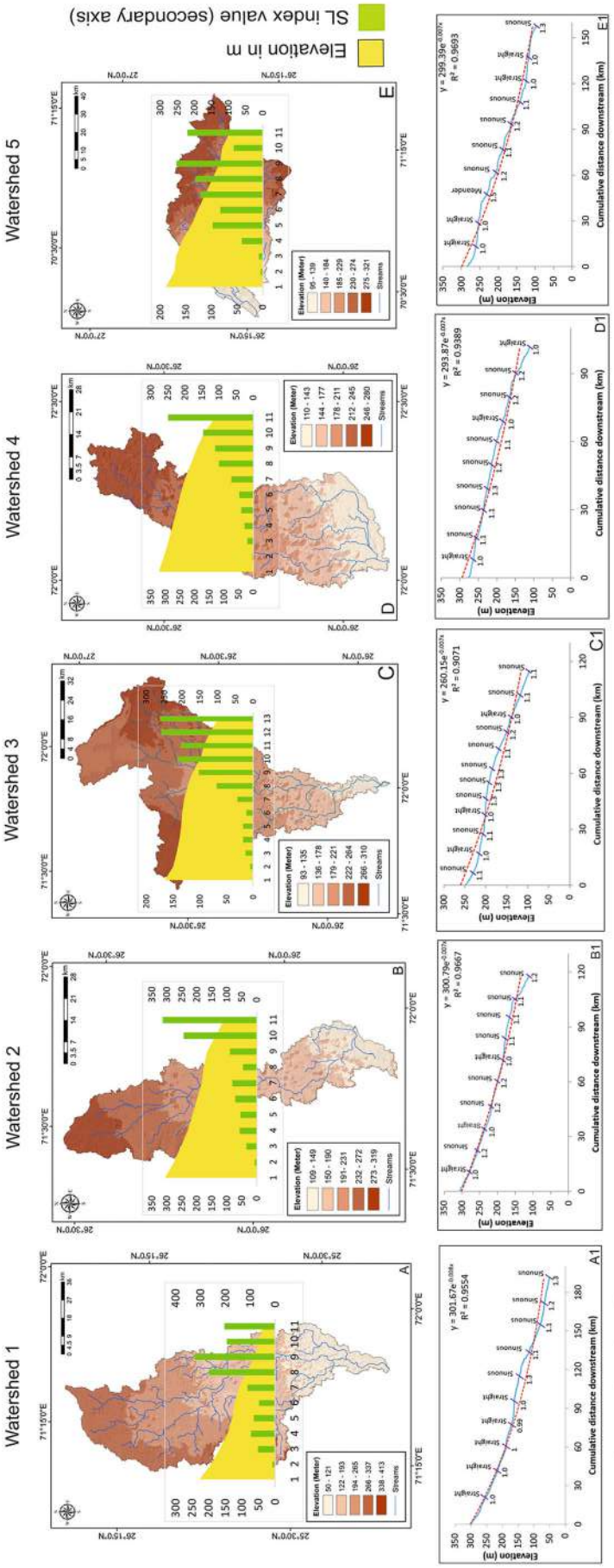

Figure 4. **(A–E)** Graphical representation of stream length gradient index (SL) in respect of elevation of watersheds 1, 2, 3, 4 and 5, respectively. **(A1–E1)** Exponential curve fit and R^2 values along the long profiles of the watersheds 1, 2, 3, 4 and 5 with detailed sinuous characteristics from source to mouth.

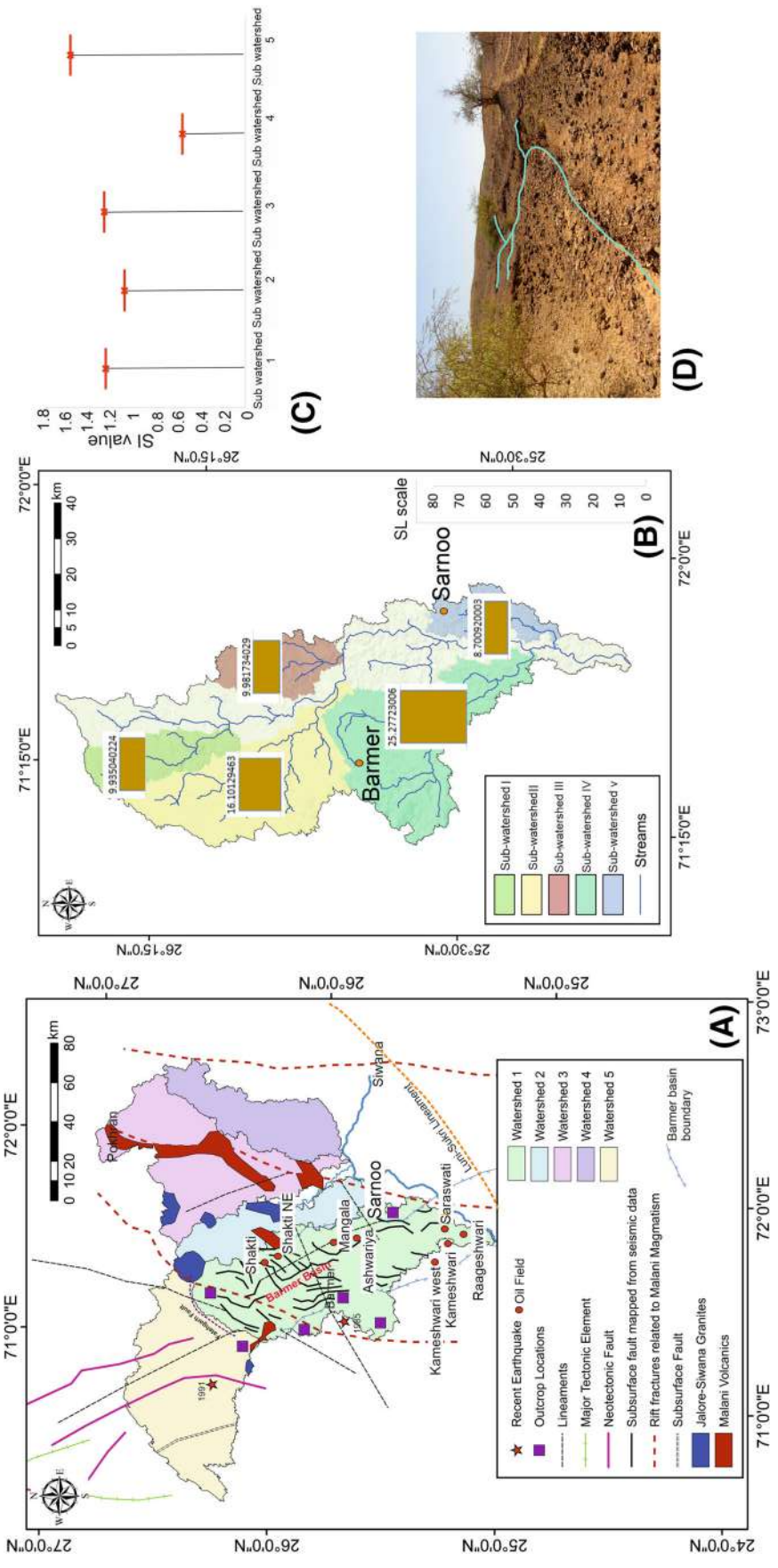

Figure 5. (**A**) Detailed geology and alignment fault lines and fractures over the watersheds. (**B**) Sub-watershed delineation of tectonically active watershed-1 with bar graph of SL indices for the five sub-watersheds. (**C**) Sinuosity index of the sub-basins where sub-watersheds 4 is of straight, 1 and 3 are sinuous, and 5 is meander pattern. (**D**) Image of small catchment of sub-watershed 1 near the Fatehgarh fault where the consequent river is straight as per SI.

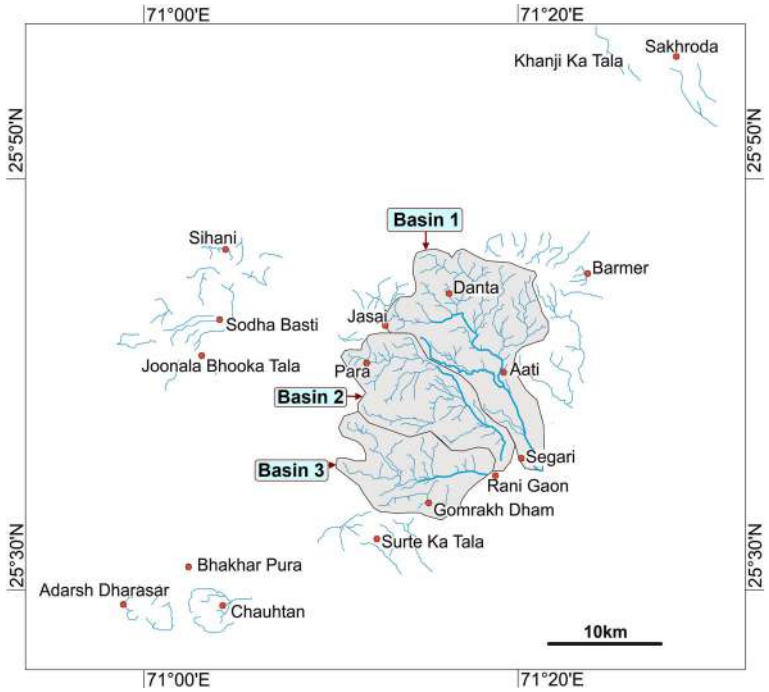

Figure 6. Dry gully systems identified around Barmer are divided into three basins (1, 2 and 3) around. Basin-1 located around Danta and Aati, basin-2 is located between Para and Rani Gaon, and basin-3 is located around north of Gomrakh Dham area.

Table 2. *Results of basin asymmetry factor (AF) analyses of three basins around Barmer.*

Basins	Ar (km^2)	At (km^2)	Drainage basin asymmetry (AF) $AF = 100\times(\frac{Ar}{At})$
1	72	146.75	49.06
2	24	93.63	25.63
3	40	78.66	50.85

(Mahmood and Gloaguen 2012). These parameters are ranked according to the actual values of each considered watershed and finally, IAT is calculated and classified (figure 3A, B). The resulted from IAT values are categorized into three ranges, which vary from 1.28 to 1.88 under class-1 (high), 1.89–2.49 under class-2 (moderate), and 2.50–3.10 within class-3 (low) (figure 3C). Watersheds 1 and 2 are highly active as their IAT values belong to class-1. Watershed 4 and 5 are moderately active (class-2), whereas watershed-3 is less active (class-3) (figure 3D).

Besides the spatial-scale indicators, the linear aspects of streams specify the active tectonics. We estimate stream length gradient index (SL) and sinuosity index (SI) for individual watersheds. The SL identifies the anomalous knick-points along the river with respect to elevation from source to mouth. The calculated and plotted lower SL values in the upper section of watershed-1 in

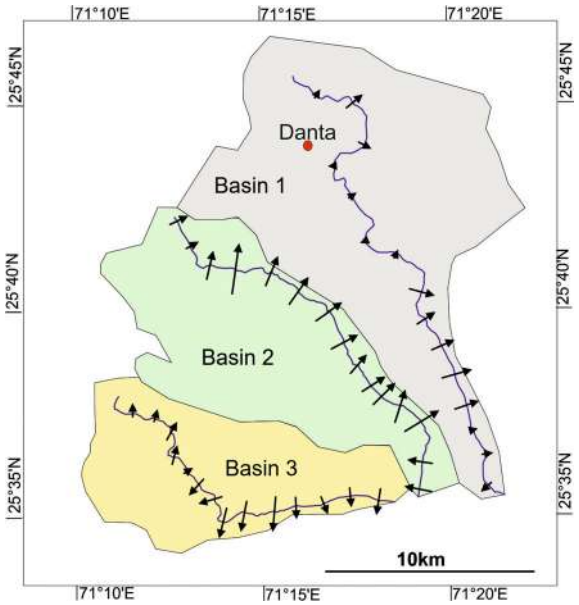

Figure 7. Basin asymmetry factors with magnitudes given in table 2 obtained from transverse topographic symmetry analyses of basins 1, 2 and 3 as shown in figure 6.

figure 4(A) indicate that the area is tectonically active. The values increase towards the south and decrease towards the lower course of the channel due to another SW–NE aligned lineaments near Sarnoo. In figure 4(A1), SI is compared along with the long profile with channel characteristics changing from straight to sinuous.

Table 3. *Results of valley floor width to height ratio (V_{fwh}) for main gullies basns 1, 2 and 3 of the Barmer area.*

Basin	Locations (Lat/Lon)	Variables	Results (V_{fwh}) $2V_{fw}/[(E_{ld} - E_{rd}) + (E_{rd} - E_{sc})]$
1	25°44′27.9443″N	V_{fw} = 166 m, E_{ld} = 169 m	94.86
	71°17′56.4827″E	E_{rd} = 168 m, E_{sc} = 165.5 m	
	25°42′44.8585″N	V_{fw} = 211 m, E_{ld} = 154 m	105.50
	71°17′29.5103″E	E_{rd} = 153 m, E_{sc} = 150 m	
	25°42′2.4977″N	V_{fw} = 280 m, E_{ld} = 149 m	103.70
	71°18′8.2410″E	E_{rd} = 148.8 m, E_{sc} = 143.6 m	
	25°40′32.7124″N	V_{fw} = 208 m, E_{ld} = 135 m	198.10
	71°19′27.0579″E	E_{rd} = 134.6 m, E_{sc} = 132.9 m	
2	25°40′49.3789″N	V_{fw} = 239 m, E_{ld} = 161 m	239.00
	71°15′8.5307″E	E_{rd} = 161 m, E_{sc} = 159 m	
	25°39′49.8865″N	V_{fw} = 260 m, E_{ld} = 142 m	173.33
	71°17′2.5975″E	E_{rd} = 141 m, E_{sc} = 139 m	
	25°38′17.8105″N	V_{fw} = 287 m, E_{ld} = 128 m	143.50
	71°17′53.8029″E	E_{rd} = 135 m, E_{sc} = 124 m	
	25°36′50.3149″N	V_{fw} = 332 m, E_{ld} = 113 m	664.00
	71°19′35.4347″E	E_{rd} = 118 m, E_{sc} = 112 m	
3	25°36′21.3857″N	V_{fw} = 273 m, E_{ld} = 185 m	45.50
	71°12′43.3560″E	E_{rd} = 182 m, E_{sc} = 173 m	
	25°35′10.7628″N	V_{fw} = 236 m, E_{ld} = 136 m	94.40
	71°13′56.9714″E	E_{rd} = 132 m, E_{sc} = 131 m	
	25°35′8.0349″N	V_{fw} = 188 m, E_{ld} = 114 m	188.00
	71°15′32.0065″E	E_{rd} = 113 m, E_{sc} = 112 m	
	25°35′20.6964″N	V_{fw} = 344 m, E_{ld} = 113 m	83.50
	71°17′51.9031″E	E_{rd} = 106 m, E_{sc} = 105 m	

Table 4. *Results of sinuosity index (SI) of main gullies of the basins 1, 2 and 3.*

Main gully of	Variables (km)	Sinuosity index $SI{=}CL/VL$
Basin 1	CL=19/ VL=16.67	1.14
Basin 2	CL=19.37/ VL=15.12	1.28
Basin 3	CL=12.4/ VL=9.7	1.27

In watershed-2, changed SL values in the upper section of the channel indicate active tectonics (figure 4B). The SL values are compared with the sinuosity values in figure 4(B1). Alteration of lower SL values and aligning nature (straight to sinuous and sinuous to straight) of the channel signifies the watershed to be tectonically active. But comparing watersheds-3 and 4, a regular increase in SL values towards low elevation in the lower course of the channels and upper course of the catchments are noted. Most of the points along the channel are sinuous (figure 4C, C1, D, D1). The higher SL values along the channels indicate variable lithology and thrusts (Sharma *et al.* 2018) and the lower values of SI indicate deep vertical cutting due to faulting (e.g., Dehbozorgi *et al.* 2010). The regular pattern of increased values of SI is associated with less disturbances and alterations with uplift/incision and aggradation/degradation sequences of the channel. In watershed-5, the channel significantly experiences tectonic disturbances (e.g., the 1995 seismicity; figure 4E, E1). The alternative changes of SL values are compared with the SI value of the same points. If we compare the R^2 and exponential curve fit of the watersheds, all are indicating tectonic activeness of the watersheds.

Changes in SL values denote straight to sinuous and sinuous to straight channel patterns towards downstream specifying the channel geometric

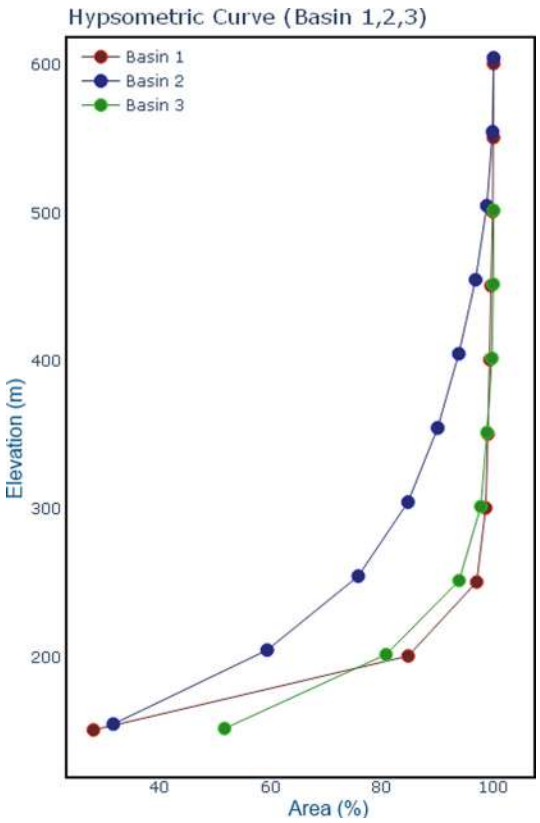

Figure 8. Hypsometric curves of three basins plotted as elevations of corresponding basins *vs.* the percentage of basin area.

anomalies originating from the Fatehgarh Fault zone. Flowing towards the west, the channel passes through the neotectonic fault zone (NNW–SSW and NNW–SSE) and lineaments (SSW–NNE). We note that most of the oil fields, e.g., Shakti, Shakti NE, Mangla, Ashwariya, Saraswarti, Kameshwari, Kameswari west and Raageshwari are located in watershed-1, which is tectonically active as indicated by its low IAT value (figure 5A).

Sub-watershed analysis. Linear aspects of geomorphology as stated in the previous section are applied on the sub-watershed-1, where five sub-watersheds are defined (figure 5B). For each sub-watersheds, SL and SI (figure 5C) have been calculated. The results distinctly verify the minimum SL value in sub-watershed V due to SW–NE trending lineament and faults near Sarnoo. It is followed by sub-watersheds I and III. Sub-watershed I originate from the southward-sloped section of the Fatehgarh Fault (figure 5D). Similarly, in sub-watershed III, the sub-surface faults along with the eastward border of the rift basin have controlled the channel flow lines. Higher SL values of sub-watersheds II and IV signify tectonic control. Most of the subsurface fault lines and rift fractures are alighted in sub-watershed II near the Giral coal mine area (Dasgupta and Mukherjee 2017). Here the channels flow parallel or across the fault lines in a straight manner that promoted more vertical than lateral erosion (figure 5A).

The SI index comparatively displays sinuous to straight nature except in sub-watershed V. This sub-watershed has low SL and high SI, which denote meandering channel path. We indeed note an incised meandering channel, controlled by structure and fault lines. The hill is composed of sandstones, which enables lateral erosion than granites or rhyolites (figure 5B, C).

5.1 *Morphology of micro-basin in western section of Barmer*

With the macro and meso-scale spot study, micro-basin morphotectonics of the Jaisalmer–Barmer area reveal the presence of some dry gully valleys in and around the Barmer and the Chautan area. The Barmer section belongs to the highly tectonic (IAT) in watershed-1 where gullies at Chauhtan area are annular and controlled by domal morphology of the rock outcrops. Gullies observed near Sihani and Sodha Bastiare are radial. Three prominent dendritic gully systems occur near the Barmer area: basins 1–3 (figure 6).

5.1.1 *Morphometric analyses of basins of the Barmer area*

Table 2 presents asymmetry (AF) analyses (Hare and Gardner 1985; Keller and Pinter 2002) of basins 1–3 as shown in figure 7. Analyses indicate that basin 2 has an unstable ground setting compared to basins 1 and 3. AF values for basins 1 and 3 are ∼50. AF gives significant clue of active tectonics (Dhanya 2014), hence the ground instability may be related to the few NW–SE trending lineaments (L21–23) located at watershed-2.

Valley floor to height ratio (V_{fwh}; Bull and McFadden 1977) shows the localized conditions of the channel, which depends on the presence of resistant rocks or due to the presence of structural features. Table 3 presents V_{fwh} analyzed for main gullies for each basin. It is observed that the main gullies of basin-2 have narrow valley in mid-segment indicating rapid incision. Similarly, the gully of basin-3 has narrow valley upstream due to flow along structural lineament (table 3).

Table 5. *Results of hypsometric curve analyses calculated from change in elevation (in m) with respect to percentage of area of the basins 1, 2 and 3.*

Area (%)	Elevation (m)
Basin 1	
28.18	151
84.68	201
96.96	251
98.58	301
98.99	351
99.35	401
99.55	451
99.85	501
99.97	551
100	601
Basin 2	
31.73	155
59.35	205
75.71	255
84.64	305
89.96	355
93.74	405
96.77	455
98.78	505
99.82	555
100	605
Basin 3	
51.71	152
80.71	202
93.80	252
97.70	302
98.82	352
99.70	402
99.94	452
100	502

Sinuosity index (SI; Brice 1964; Horacio 2014) analysed for main gullies of all three basins are presented in table 3. SI values range between 1.14 and 1.27. Sub-basin's/sub-watershed's SI and SL are presented in table 4.

Hypsometric curve analyses (Zävoianu 1985; table 4a–d; figure 8) give the idea of relative elevations of a particular percentage of areas of basins. It is observed that 98% of the area of basin 1, 84% of the area of basin 2 and 97% of the area of basin 3 are under 300 m. Alternately, it can also be concluded that sources or heads of these gullies are located at up-lands, but mid bodies and toes of these gullies are located in valleys. Therefore, basin-2 has more uplands compared to the other two watersheds (figure 8). Topographic symmetry factor (Cox 1994) analyses the effects of active tectonics over the micro-fluvial basins. The ratio between *Da* (length measured from basin midline to stream midline) and *Dd* (length measured from basin midline to basin divide) was calculated for watersheds 1–3 (table 5). The factor indicates shift of gullies from the basin mid-lines, which may be due to tectonic control. Main gully of watershed-2 shows northward shift with minor shift in the gully of watershed-3 at south. Lower part of the main gully of the watershed-1 is parallel to the northward shift (table 6).

Normalized longitudinal profile analyses (e.g., Ayaz *et al.* 2018; Biswas and Paul 2021) were done for main gullies of basins 1, 2 and 3. These profiles were fitted with linear and exponential regression curves (figure 9, table 6) to understand the incision

Table 6. *Results of transverse topographic symmetry (T) analyses of basins 1, 2 and 3.*

Basin 1			Basin 2			Basin 3		
Da	*Dd*	*T*	*Da*	*Dd*	*T*	*Da*	*Dd*	*T*
0.47	1.30	0.36	1.36	1.58	0.86	0.90	1.20	0.75
0.14	0.76	0.18	0.62	1.36	0.46	0.80	1.35	0.59
0.09	0.93	0.10	0.73	1.46	0.50	0.70	1.42	0.49
0.53	0.99	0.54	1.19	1.60	0.74	0.80	1.45	0.55
0.69	1.03	0.67	1.25	1.68	0.74	1.03	1.42	0.73
0.61	1.50	0.41	1.00	1.75	0.57	1.01	1.40	0.72
0.89	2.20	0.40	1.17	2.06	0.57	1.22	1.97	0.62
1.50	3.20	0.47	1.48	2.61	0.57	1.27	2.26	0.56
0.91	6.90	0.13	2.17	2.96	0.73	1.44	2.89	0.50
0.15	4.07	0.04	2.66	3.08	0.86	0.78	3.84	0.20
0.50	6.78	0.07	2.49	2.92	0.85	0.47	3.83	0.12
0.45	5.23	0.09	2.50	2.79	0.90	0.79	2.37	0.33
1.45	7.12	0.20	1.77	3.00	0.59	0.92	2.07	0.44
1.76	5.85	0.30	1.08	3.50	0.31	0.50	1.80	0.28
0.80	4.15	0.19	1.30	2.79	0.47	0.34	1.69	0.20

and deposition in these gullies. Regression coefficients (R^2) show close fit to the normalized long-profiles of basin 1, which indicates lack of significant shift in the gradient of gully. However, in case of basins 2 and 3, significant control of structural features has been observed at the upstream. Break of slope along the long-profile at midstream below regression curves indicates significant vertical erosion. Lower part of the basin shows deposition of sediments eroding from upstream and midstream segments (table 7; figure 9).

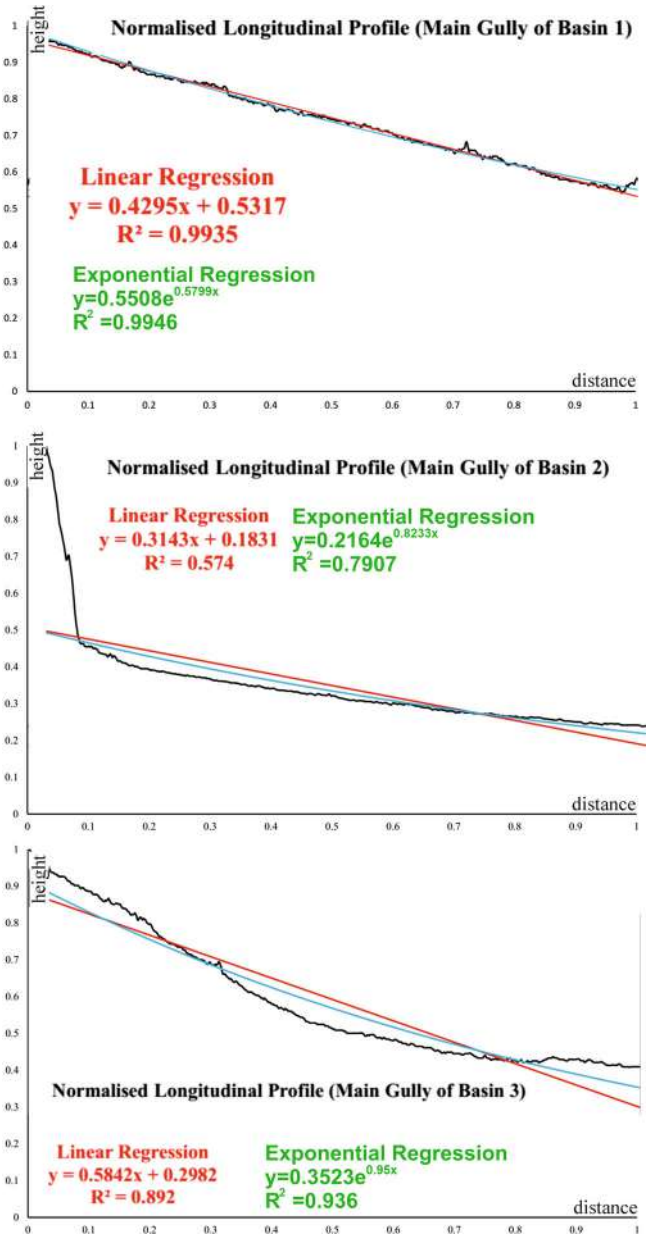

Figure 9. Normalized longitudinal profiles of chief gullies of basins 1, 2 and 3 are presented along with equations and R^2 values of linear and exponential regression analyses.

5.2 *Field verification and observation*

Using the IAT results, we classified the watersheds into three grades as high, moderate, and low. These parameters have been applied regionally and act decisively in landform development (Czerniawska and Chlachula 2017). To validate the discussed observations, field-based micro-scale data of five concerned points from watersheds-1 and 2 have been surveyed. Overall the surveys show a strong correlation with structural discontinuities, geomorphologic anomalies and alternating valley characteristics.

5.2.1 *Fatehgarh fault area (26°26′55.68″N/71°14′7.81″E)*

The northernmost part of watershed 1 (figure 10A, B) consists of numerous gullies and rills that are coming down towards the south with deep incisions and vertical valleys cutting almost orthogonally. These drainage lines are mostly straight with SI < 1.0.

Two first-order streams have been selected to study their valley sections from source to the local base level where they join the 2nd order stream. As in figure 10(C), the stream cut ∼1 m vertically. The incision anomalies are well distinguished comparing the section from (d) to (h) in figure 10(D). Near the source, the wide valley depicts more lateral erosion while towards downstream it becomes narrow and deep alternatively. Sections (i) and (j) commonly represent 'V' valley geometry. The valley width/depth ratio suddenly decreases to 1 towards downstream and again increases to 1.7 near the confluence. Changes in W/H ratio within a short distance indicate

Table 7. *Linear and exponential regression analyses of normalised longitudinal profiles of basins 1, 2 and 3.*

Basin	Linear regression (y=mx+b)	Exponential ($y = ae^{bx}$)
1	$y = 0.4295x + 0.5317$, $R^2 = 0.9935$	$y = 0.5508e^{0.5799x}$, $R^2 = 0.9946$
2	$y = 0.3143x + 0.1831$, $R^2 = 0.574$	$y = 0.2164e^{0.8233x}$, $R^2 = 0.7907$
3	$y = 0.5842x + 0.2982$, $R^2 = 0.892$	$y = 0.3523e^{0.95x}$, $R^2 = 0.936$

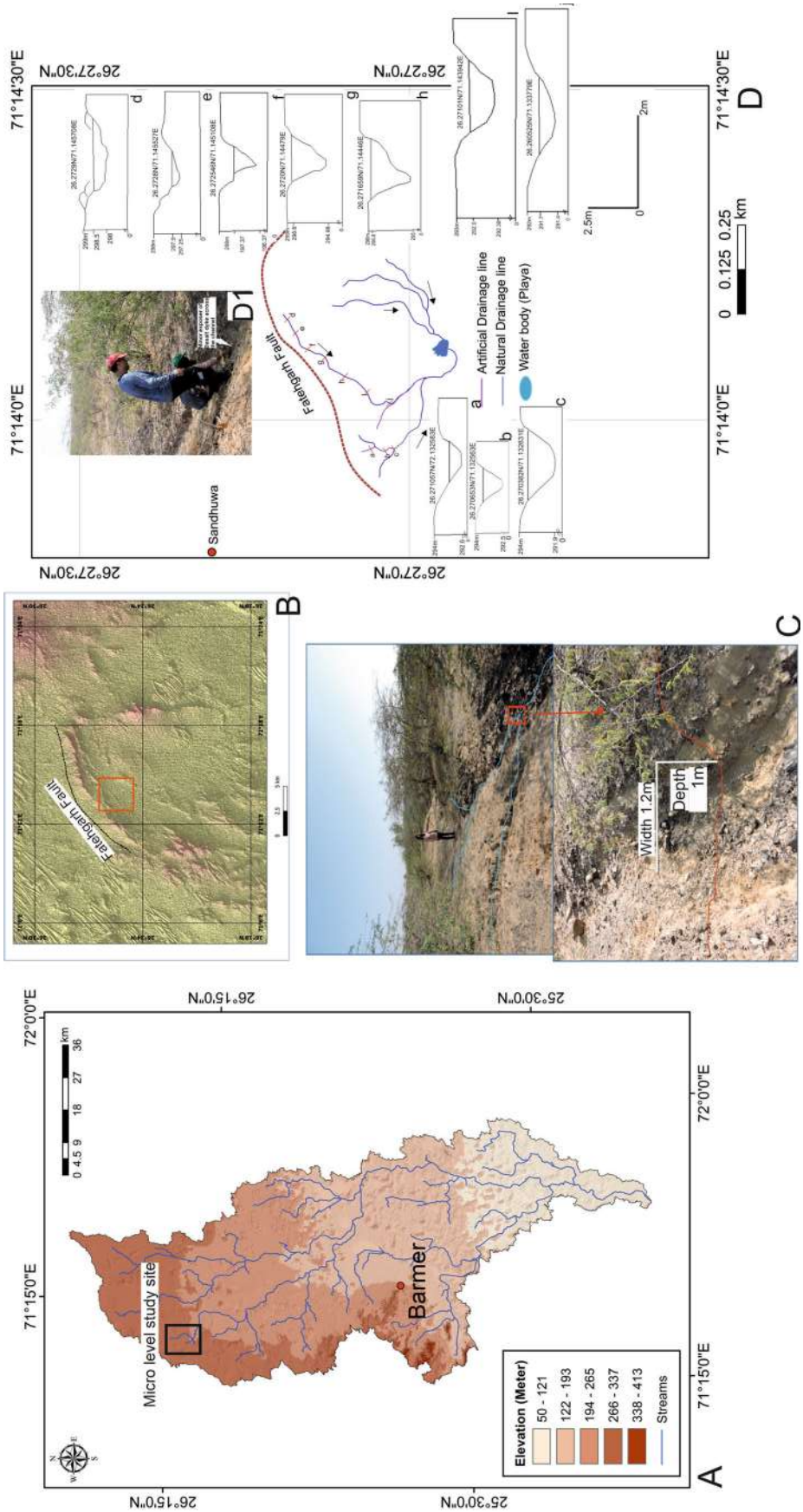

Figure 10. **(A)** Location of micro-level field study site of watershed-1. **(B)** Fatehgarh Fault area and its adjacent relief features with the study site of gully channels (red marked). **(C)** Field photos of studied gully channel, deeply incised ~ 1 m depth. Inset: two tributaries join along NNE–SSW. **(D)** Ten surveyed cross-sections of two gullies point out in the map where one natural water body exists as playa. **(D1)** Exposed basalt dyke in the river bed due to vertical incision near cross-section 'h'.

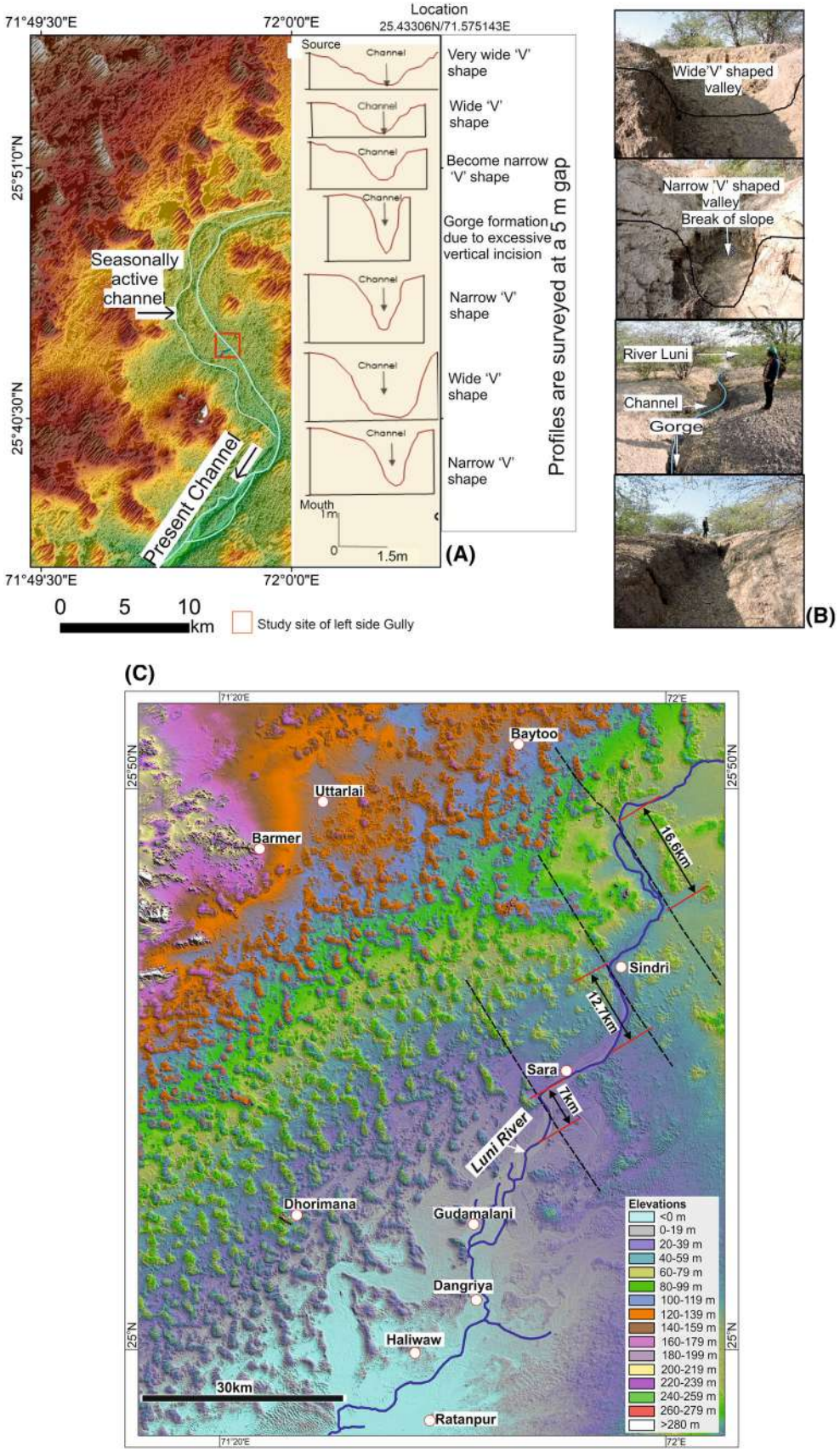

Figure 11. (**A**) Field-based six cross-sections of a gully from source to mouth (meeting point with Lini/Sukri) with detailed inset map of the seasonally active channel and the main channel. Red box: location of the studied gully. (**B**) Different V-shaped valleys of the gully, also wide to narrow and gorge 'I' shape valley present. (**C**) River offset observed in Luni River near Sindri and Sara area resulted from NW–SE strike-slip movement of 7, 12.7 and 16.6 km, respectively.

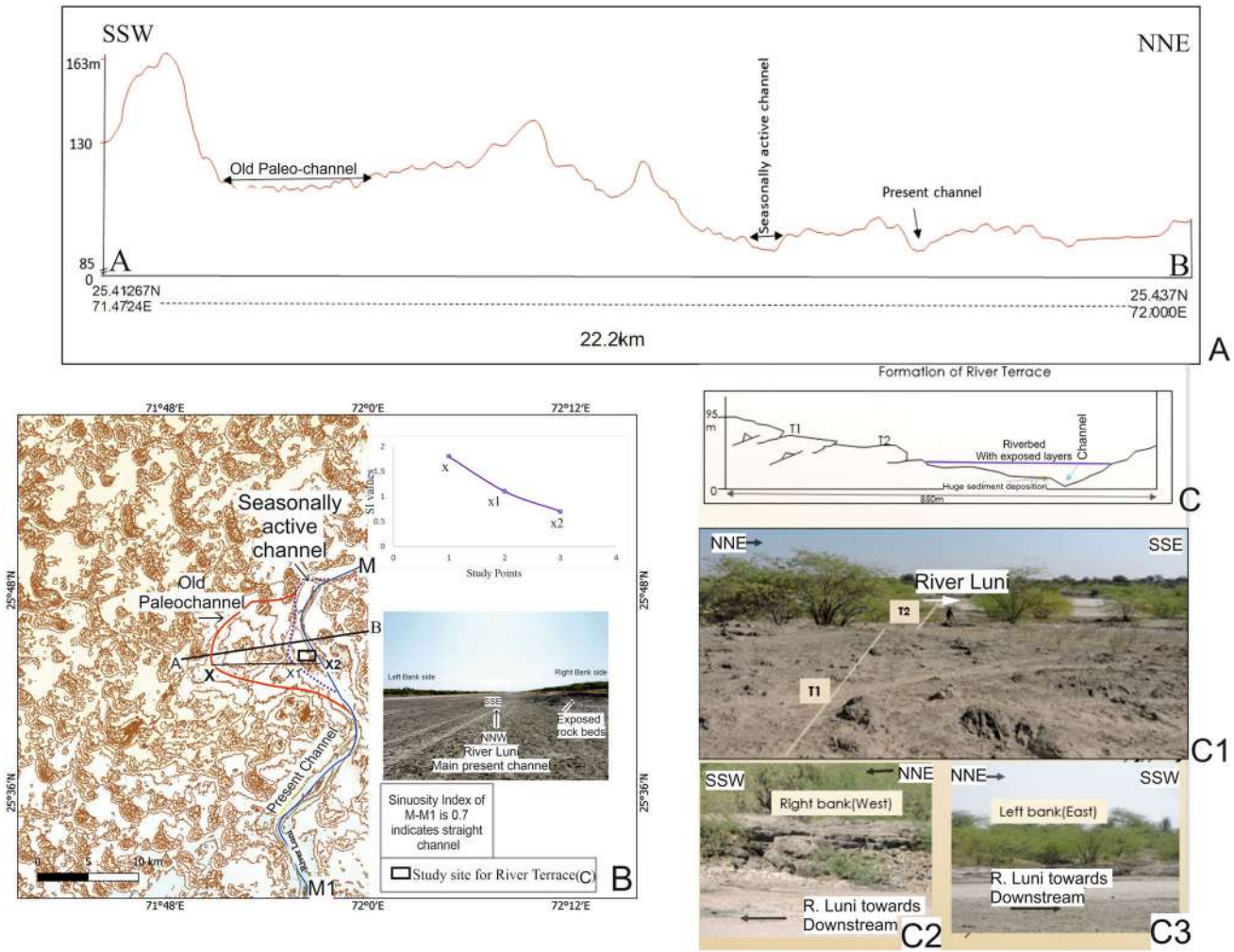

Figure 12. **(A)** Relief section of 22.2 km from SSW–NNE (line AB; from figure 10B). Specifically, a paleo-channel, a seasonally active channel and a present channel marked. **(B)** 'x–x2' is the considered line to calculate sinuosity index from old paleo-channel to present. Along the longitudinal distance 'M-M1' (present channel) sinuosity index has been calculated as 0.7. Line graph of decreased values of SI from 'x' to 'x2' indicates changes of channel pattern from sinuous to straight. **(C)** Two-tier river terraces of the main channel. **(C1)** T1 and T2 are evident as the rejuvenation of the river with photographic evidence of the terraces mainly composed of basalt. **(C2, C3)** Distinctly exposed rocks in two banks of the river where river has incised ∼90°.

structural control on gully streamlines. One does find basalt dykes exposed in the channel bed (figure 10D1). Intense vertical cutting with SI values 0.7, 0.8, 0.9 and 1.1 between d–e, e–f, f–g and g–h, respectively, indicate that the area is weaker and composed of fragile weathered rocks (sandstones). Thus, minor streams eroded the rocks.

5.2.2 *Sukri/Luni river (25°43′48.15″N/ 71°57′0.87″E):*

Numerous gullies join the accurate channel anomalies from source to mouth along NNW–SSW. These are characterized by prominent alteration of valley shape and incision in the form of adequate superimposition of ∼90° valley side-cutting. Figure 11(A) displays the abandoned channel of the Sukri/Luni River that has shifted towards the east. Two prominent channels are considered. Amongst them, one is seasonal and the other one is noted as the present channel. Presently (Feb-2021), the channel is dry and zig/zag with salt-deposition lines within the bed staying as remnant. Figure 11(B) is the sequential section of the gully cross-profile from source to mouth representing strong anomalies in valley shape (very wide V, wide V, narrow V, gorge, narrow V, wide V to narrow V shape, at each cross-section). This shape alteration indicates tectonic activities. Figure 11(B) shows valley anomalies with a recognized

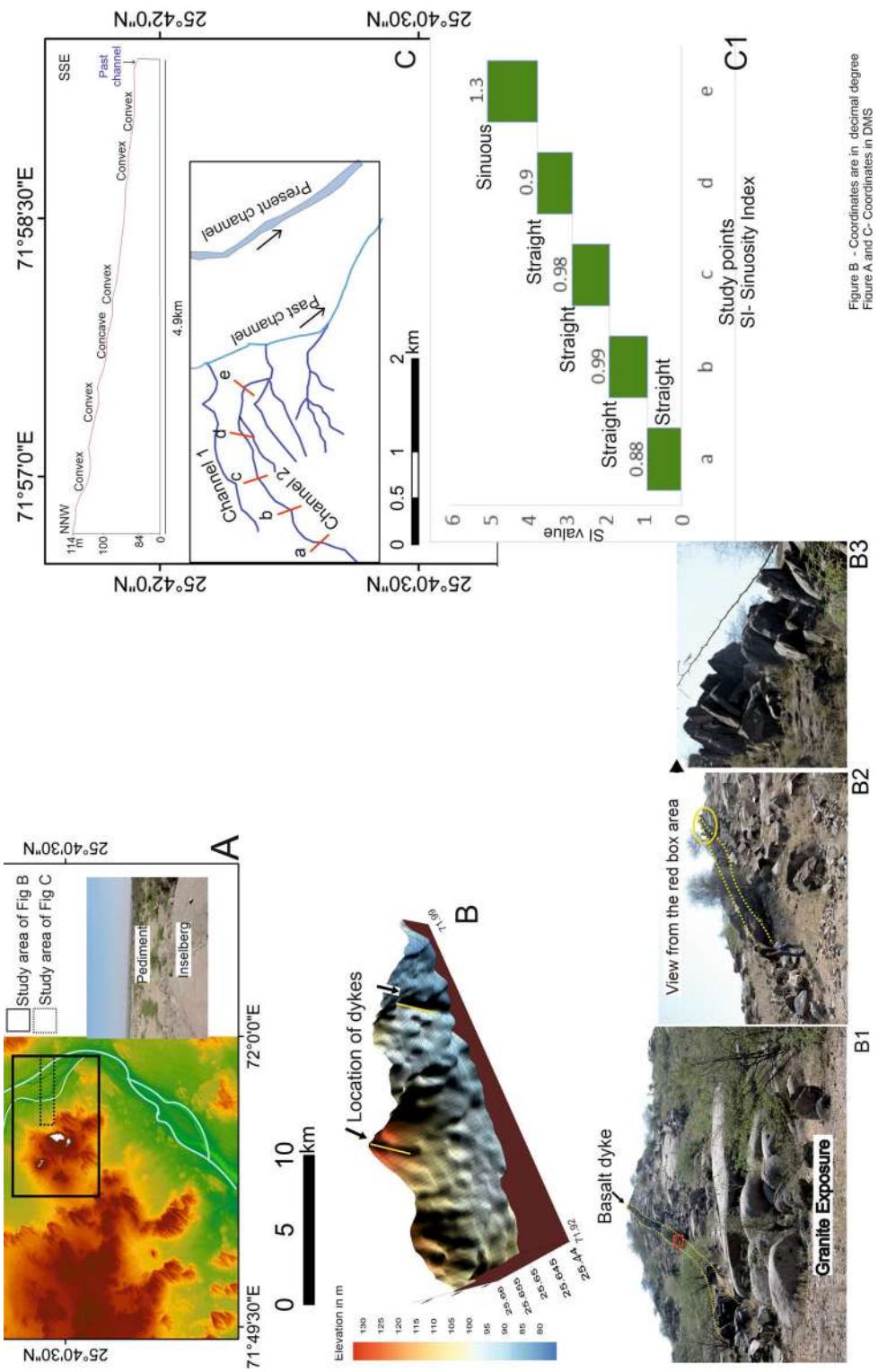

Figure 13. (**A**) Location of the field study point near Gangli in Google Earth with its adjacent area. (**A1**) Black boxes: study locations for figures (**B** and **C**). The photo view of the area distinctly identifies two major arid geomorphic features as inselberg and pediment. (**B**) 3D-diagram of exposed outcrop near Gangli where two dykes visible. **B1**, **B2** and **B3**. Basalt dyke in granite outcrop. Distinct view of red box area of **B1** in image **B2**, and in **B3** the yellow box area prominently shows the basaltic blocks of the dyke. (**C**) Location of identified channel 1and 2 wherein channel 2 five points have been considered for SI index calculation and longitudinal profile analysis. Long profile of NNW–SSE channel 2 where convex/concave shape depicts the aggradation and degradation sequence. (**C1**) Graphical representation of sinuosity index values.

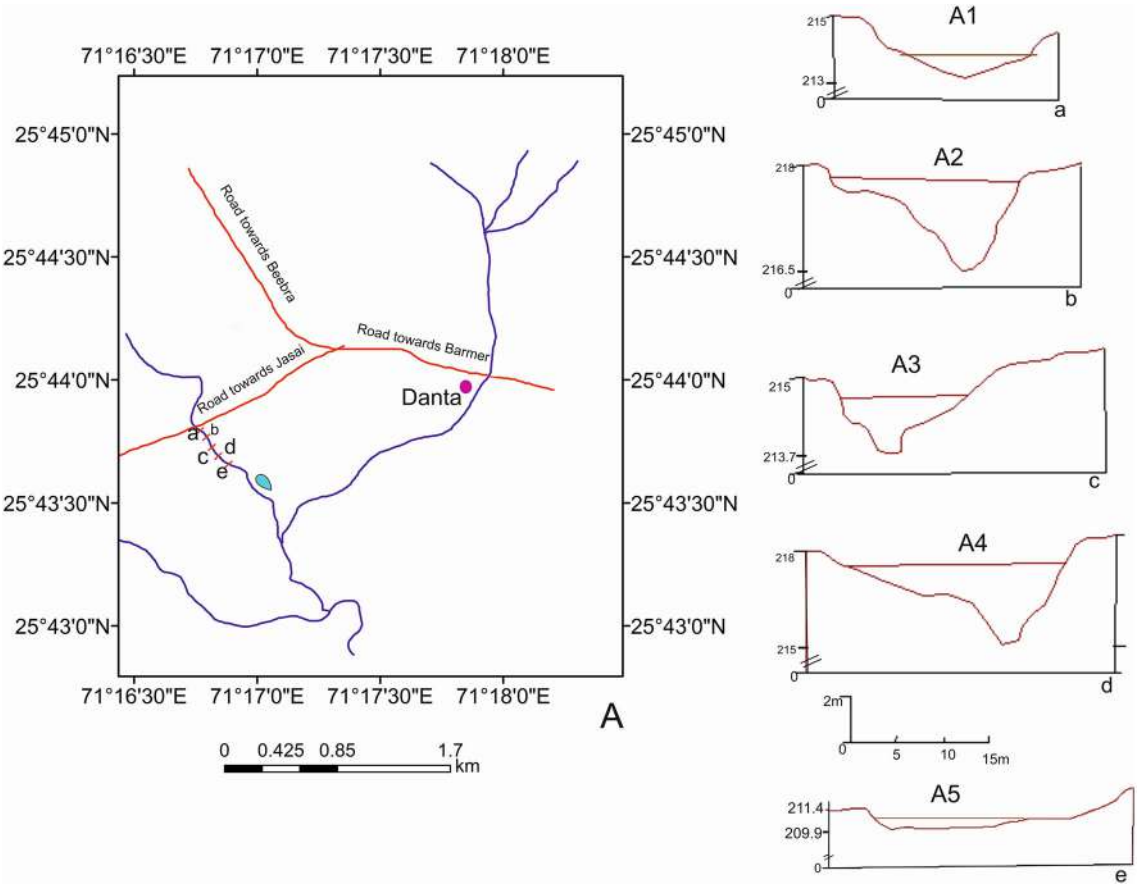

Figure 14. (**A**) Location of five cross-sections study site (a–e); **(A1–A5)** drawn valley sections. Valley side cutting ∼87°, width/depth, and incision change from A2–A4 where A3 profile is less incised and ∼67° valley side cutting.

break of the slope towards its mouth, indicating that the gully channel is more active.

Close observation (figure 11C) of Luni river towards the SE corner of the study area shows NW–SW sinistral strike–slip movements at Sindri (16.6 km), Sara (12.7 km) and Gudamalani (7 km).

Figure 12(A), based on extracted data from SRTM, portrays cross-elevation profiles from the southern section to the isolated hilly top of the Sarnoo to the present channel. We re-examined the shifted channels that point out the elevation in between them. Besides, figure 12(B) displays another paleo-channel identified from remote sensing data. Two shifting procedures have occurred in the past that have reframed the channel liner pattern. From x to x1, it shifted 7.94 km and from x1 to x2, it is 0.08 km. The cross-sections represent paleo-channel (at point x), seasonally active channel (at x1) and present channel (at x2) of Luni. This 22.2 km long SSW–NNE trending section represents the isolated hilltop in the west. After the old paleo-channel, 'till' like exposure exists as a small-scale inselberg along with the existence of small-scale dunes. The remainder sections towards the east are an undulating terrain where distinct river terraces have formed between the seasonal channel and the present channel. The demarcated lines x–x1 and x–x2 present the changes in the sinuous values. These values at x, x1 and x2 are 1.6, 0.9 and 0.5, respectively (figure 12B). The calculated sinuosity index from MM1 in figure 12(B) indicates that the channel is straight, active and with a potential for vertical erosion. It reveals a change in the channel alignment from sinuous to straight.

The calculated sinuosity index from MM1 section (figure 12B) indicates that the channel is straight, active and with a potential for vertical erosion. The dry channel of Luni in figure 12(C) shows the bank-side hard rock mainly composed of basalt with rhyolite. A two-tier river terraces formed on the right bank of the main channel. This indicates that the river is in the third cycle. The terraces are composed of granite at a 25° slope up to the bank-full stage (figure 12C1). Figure 12(C2, C3) denotes the right-angle joining of the terrace to the main channel flowing along

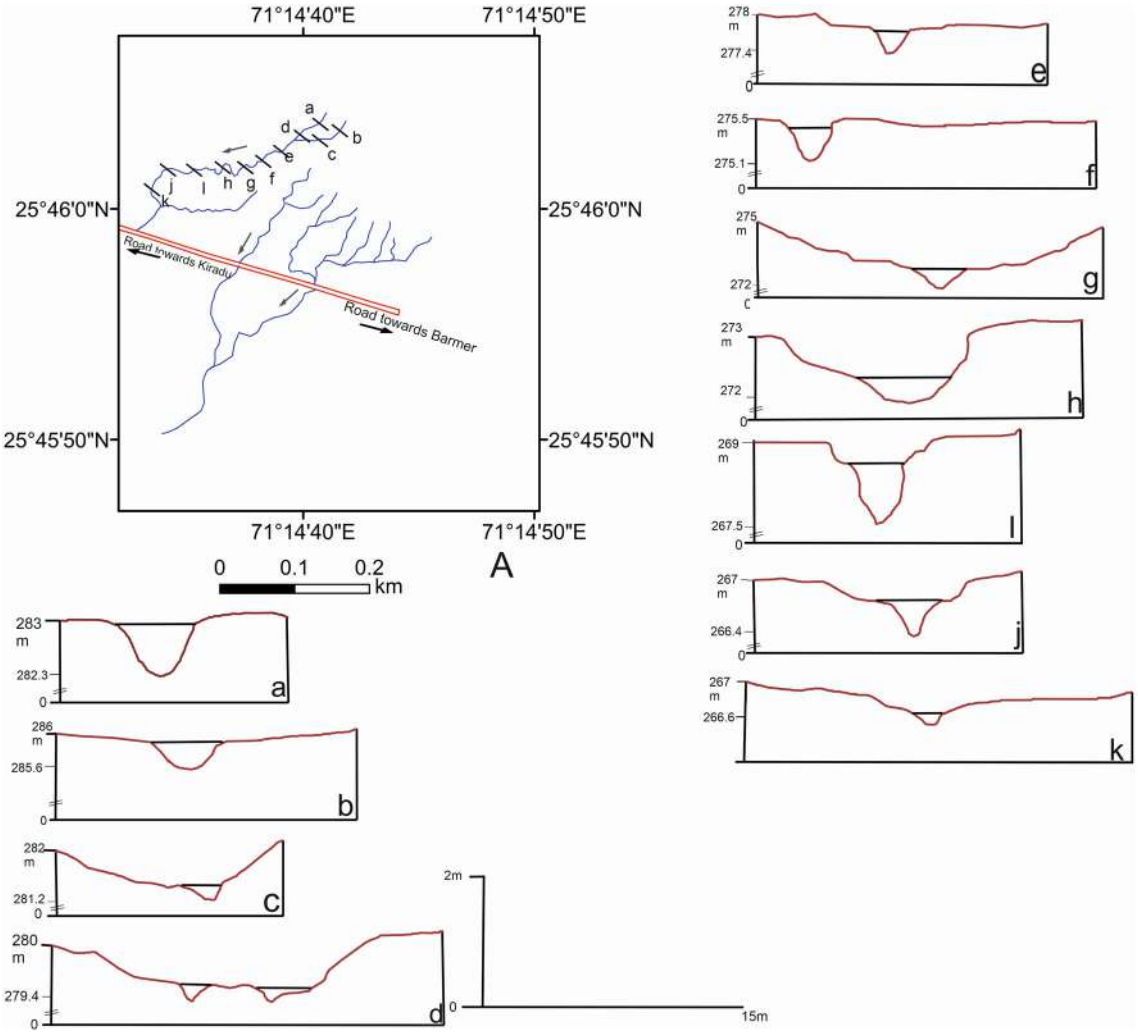

Figure 15. **(A)** Location of eleven cross-sections of a gully originated from the hilly patch of Barmer hills and flowing NNW–SSE where channel geometry changes with alteration of valley incision. **(a–k)** Valley cross-section with anomalies in incision depth and valley shape towards south. From c to g, valley is narrow; at 'h' it becomes wide due to lateral erosion and meandering has been initiated; further downstream 'I' valley with deep sub-vertical incision noted.

NNE–SSW. Both the left and right banks of the channel are granite exposures with several minor shear zones, faults and SW–NE trending exposed dykes on the riverbed.

5.2.3 *Gangli (25°41′1.21″N/71°56′31.60″E)*

It is an SSE–NNE trending elongated ridge-like granitic exposure where 'tor' like landforms and honeycomb weathering occur. A prominent channel is originated from the hilltop flowing towards the east. It follows a regional curved slope and joins Luni. This hilly ridge exhibits as an inselberg where the pediments are expanded towards the flat flood plains at a ∼2–3° to the downward slope. Figure 13(A) presents the location of the study area where two sets of analysis have been incorporated. The generated 3D view (figure 13B) of the entire section exhibits two foremost basalt dykes of 240° dip direction and 60° dip (figure 13B1, 2, 3). Between the two major channels, five points have been selected from channel-2 for channel geometry analysis based on primary survey (figure 13C). The bed elevation profile displays the convex and concave pattern alternately. The convex section of the profile represents erosive nature, whereas concave sections disclose the aggradation process. However, both are dynamic. It specifies an increase in slope and channel incision due to structural control near the confluence. The straight channel pattern of the calculated sinuosity index values (0.88, 0.99, 0.98 and 0.9; figure 13C1) determine incision process. Near confluence, though it is convex and sinuous.

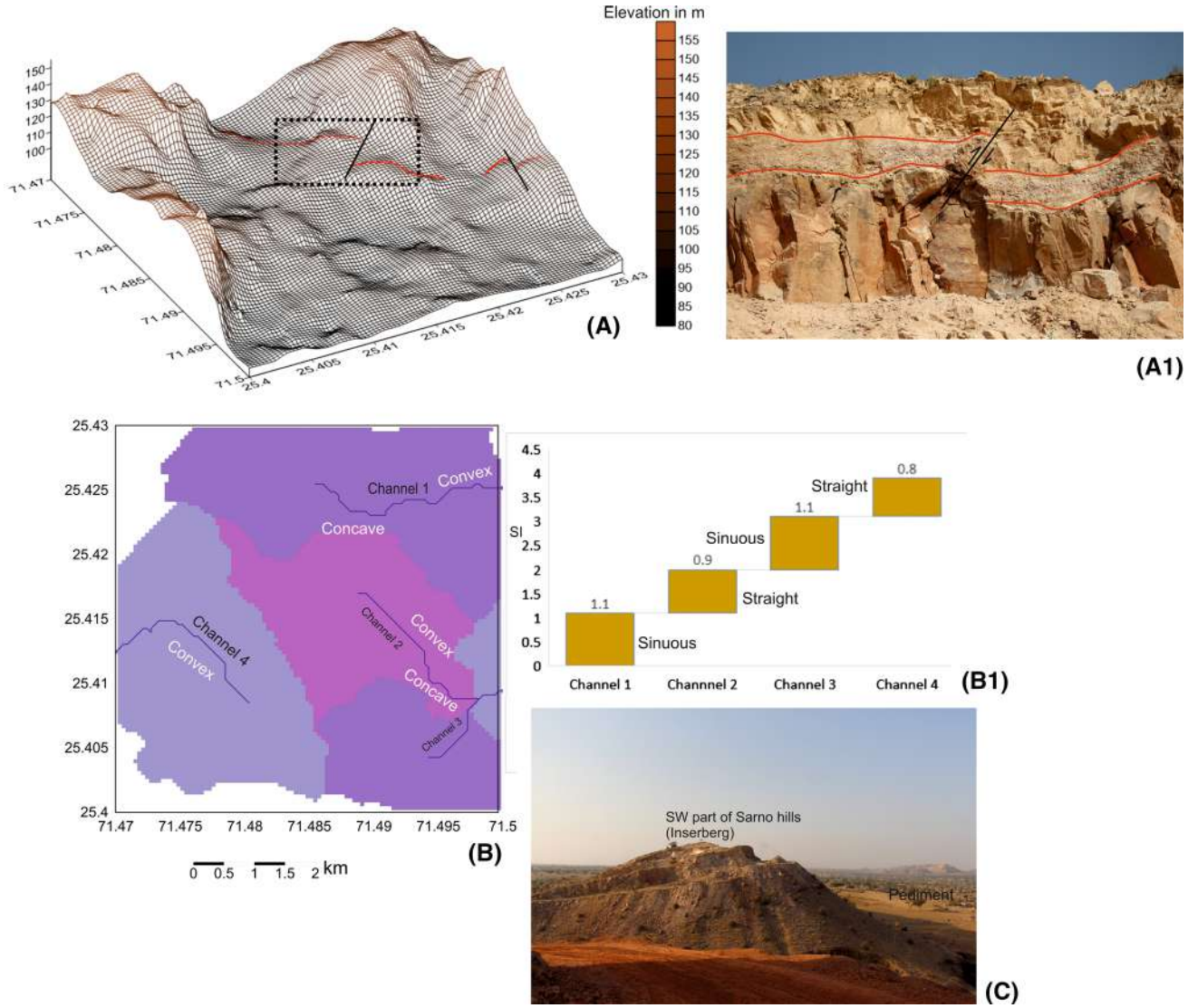

Figure 16. **(A)** Representation of Sarnoo-I elevated zone in 3D mesh layout where faults are identified and in **(A1)** field photograph of the fault. **(B)** Extracted four minor watersheds fed by four minor channels. **(B1)** Sinuosity characteristics of the channel-straight to sinuous. Two cross-sections at point 'a' and 'b' wherein 'a' channel is more incised and straight. In section 'b', valley is less vertically incised and the channel is sinuous. **(C)** Southwest part of the Sarnoo hill – an inselberg (hilly residual as remnant in the planation surface).

In the eastern section of the Barmer basin, Lower Cretaceous strata are overlain unconformably by the pre-Deccan Trap volcanic outflows. It is typified by the stratigraphic unit Tavidar Volcanic Suite with diverse compositions ranging from basalt through trachyte to rhyolite (Chenet *et al.* 2007; Sen *et al.* 2012). Sand deposited in an undulated rocky to unsorted pavements with ∼3–8° slope in the upper part and 1–3° in the middle. The lower portion representing the piedmont section has a slope of 0°8′–l° (Singh 1977).

5.2.4 *Jasai village area (25°43′34.70″N/71°16′10.91″E) and near the Kiradu temple (25°46.07″N/71°14′40.00″E)*

This study point is ∼3 km west of Danta (figure 14A) where the channels dissect the exposed granite outcrops and maintain a straight flowing path (SI < 1.0). It is controlled by the structural anomalies and SSW–NNE trending rift fractures. These fractures are probably related to the Malani rocks (Sisodia and Singh 2000). The elevated terrain with prominent outcrops (Supplementary figure 5A)

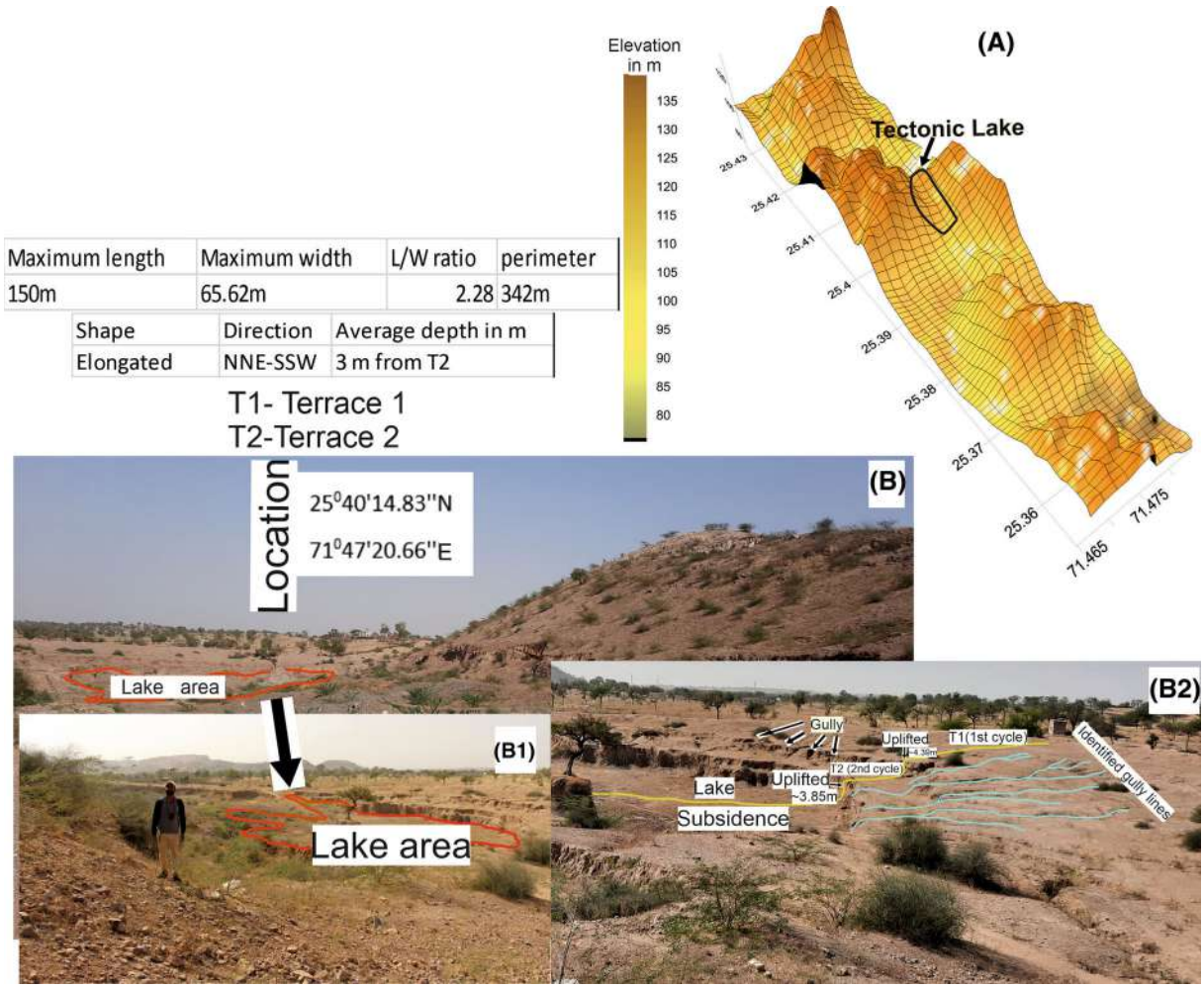

Figure 17. **(A)** Spatial 3D terrain mesh with the location of the studied lake, extracted from Cartosat 1 data. **(B)** Location and demarcation of the lake in the photograph. **(B1, B2)** Close view of the lake area and two cycles of uplift/incision notified with the formation of terraces 1 and 2. Gullies have formed surrounding the lake area over the uplifted sections.

with the contour alignment unfolds the topographic expression (Supplementary figure 5B) along with the slope directions (Supplementary figure 5C). However, this part of the study site experiences a number of tectonic events. The recent vertical down-cutting (∼87–90°) with valley shape (as wide to narrow, narrow, again narrow and then wide) anomalies towards downstream signify the uneven erosion–incision mechanism. It is associated with the changes in width/depth ratio: 10, 6, 8.3, 8 and 12, respectively, as in figure 14(A1–A5).

The study site towards Kiradu temple, near Sihani, with the same group of granites exposure, is brittle sheared (figure 15A). Numerous gullies originate from the hilly catchments. Eleven channel cross-sections along the gully that shape the channel have been noted. The gully join another streamlet to become a second-order stream flowing NNW–SSE in a straight manner with minor meandering and two breaks of slope along the channel. Figure 15(Aa–k) are the sections representing the valley shape alteration due to various incision processes. A break of slope (0.2 m) in sections (d) and (e), characterize the next two sections where intense valley deepening forms a narrow 'V'-shape. Whereas, sections (g) and (h) widen where the width to depth ratio (W/D) increases from 0.7 (f) to 20 m (h). There exists another slope break (0.62 m) after which the channel depth increases by 1.1 m with a W/D = 1.6. Uplift/incision produced a sudden break in slope. The nearby lineaments and minor fractures promoted the channel to be more erosive to reach its local base level (figure 5A). SI values define the flow-line/valley-line ratio. It changes in section (h) where the channel pattern converts from sinuous to meander as the valley becomes wide incorporating lateral expansion rather than the vertical

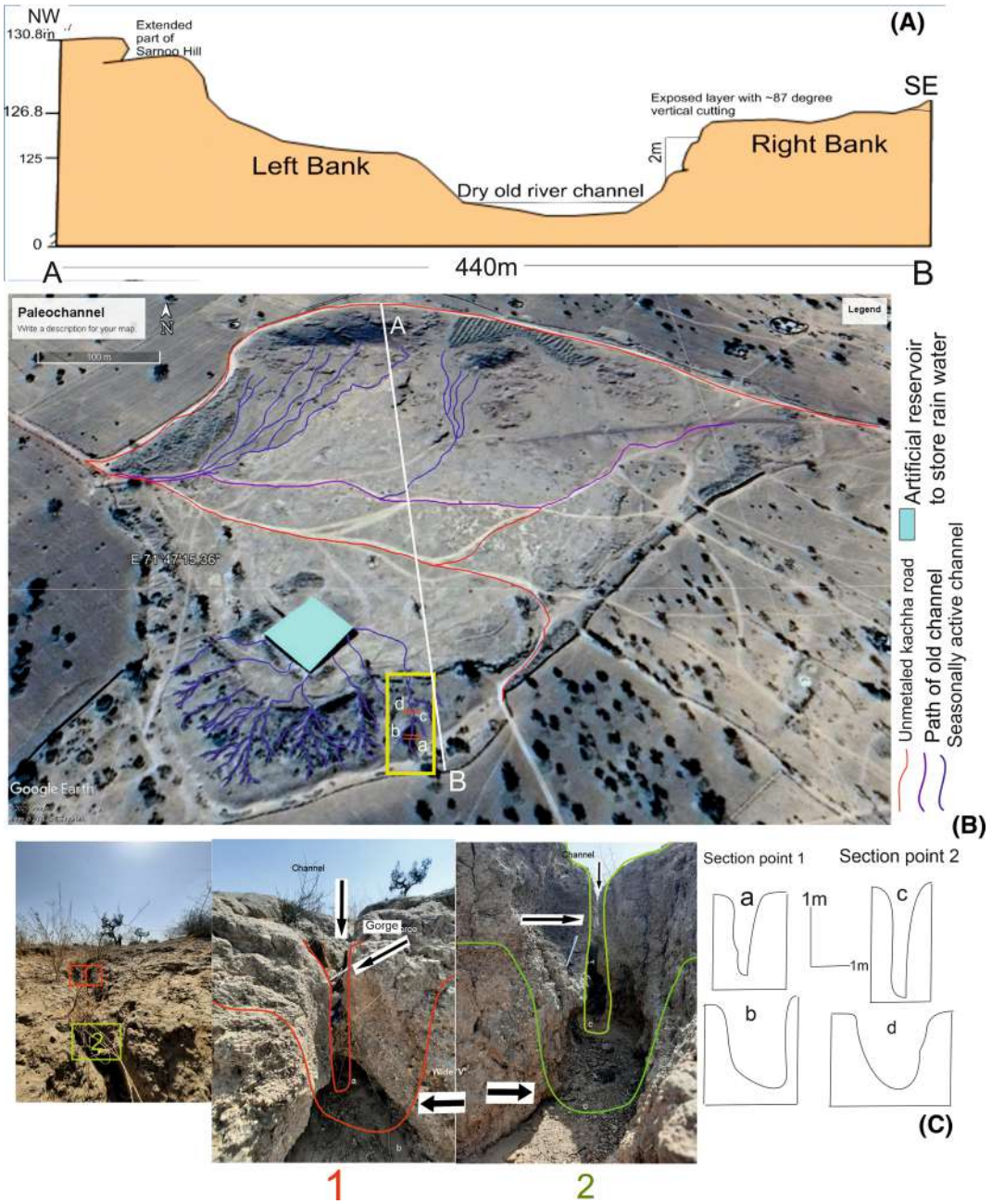

Figure 18. **(A)** NW–SE elevation section along line A–B (figure 16B) where extended Sarnoo hill towards the left bank and exposed old fluvial deposited layers in right bank side have observed with old dry river channel in between is prominent. (**B**) Old and present drainage lines (including gullies) with kachha road are marked in Google Earth image. Yellow box: four gully sections are pointed out: a, b, c and d. **(C)** Red (section point 1) and green (section point 2) boxes marked on the photo of a gully to specify the gorge and 'I' shaped valley incision of the gully channel. Measurement and plotting of gorge (section point 1) and 'I' shaped (section point 2) valleys that represent four valley sections as a, b, c and d.

incision. Nevertheless, in section (i) the value changes to 0.7, which indicates a straight channel.

5.2.5 *Sarnoo I (25°41′53.61″N/71°47′58.98″E):*

In the eastern margin of the basin, the Sarnoo hill is composed of Cretaceous Ghaggar–Hakra Formation of paleo-sediments igneous suits underlain by Malani. Previous study points of the Sarnoo area of the Lower Cretaceous is composed successively of Darjaniyon-ki-Dhani Sandstone, Sarnoo Sandstone and Nosar Sandstone (Dolson *et al.* 2015; Dasgupta and Mukherjee 2017). The extracted 3D view in figure 16(A) reveals a

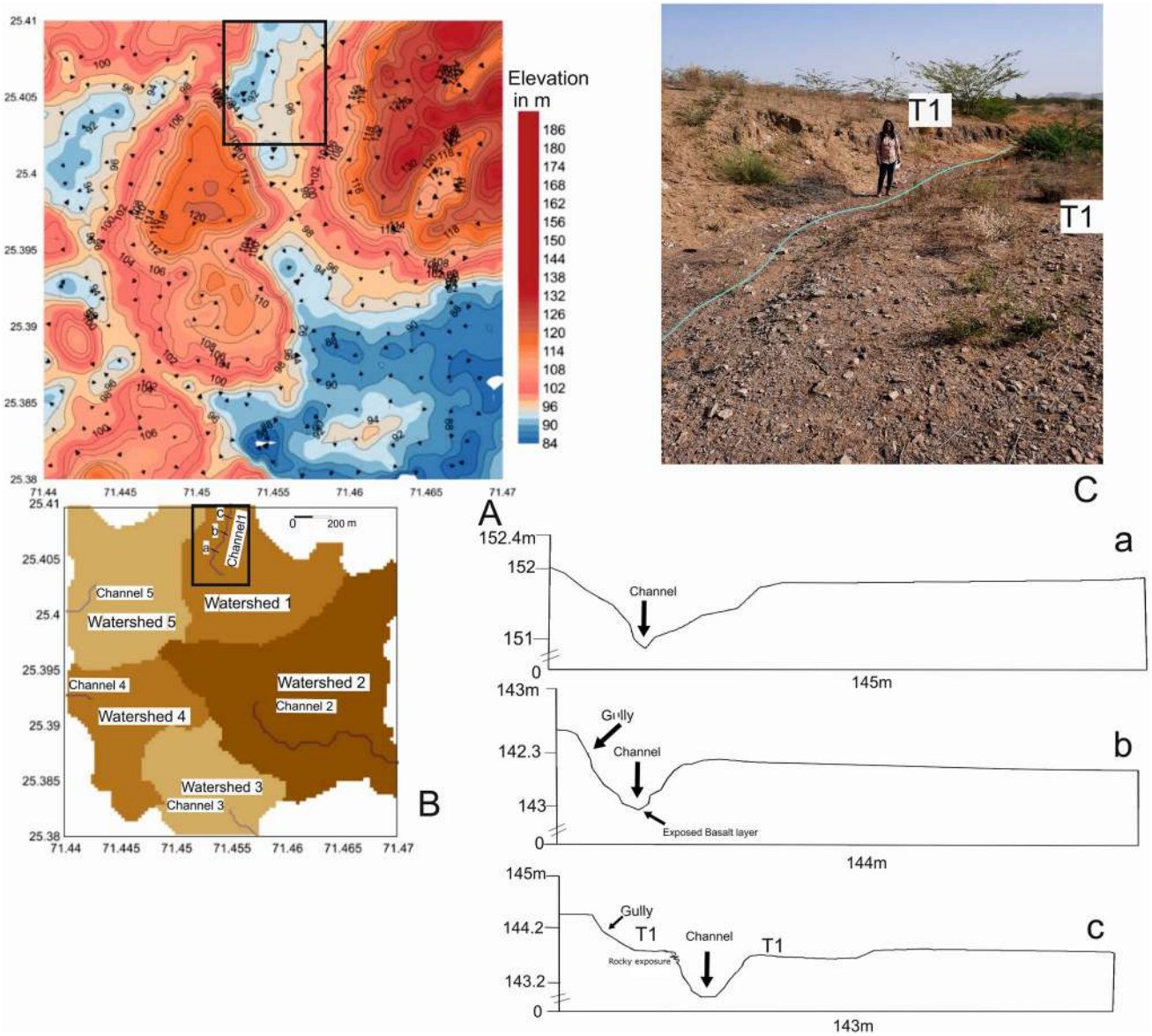

Figure 19. **(A)** Contour pattern of part of Sarnoo hills in the most southern section that represents the elevation variation and the field site is marked in black box. **(B)** Extracted five micro-watersheds around the area where five channels have been marked and the cross-valley sections have measured in three points as a, b and c in channel 1 of micro-watershed-1. Section a: Narrow 'v' valley where incision dominates by the running seasonal water due to steep slope. Section b: Valley is wide and steep side cutting at ∼86°, basalt crops out at the deepest point of the bed. Section c: Represents the T1 on both sides of the bank as unpaired terrace where sandstone is exposed on the left side edge of the T1. **(C)** Photographic evidence of T1 in both bank sides where M. Biswas faces towards SW.

prominent fault line with unconformity between Nosar and Sarnoo sandstones (figure 16A1). The fluvial system changed temporally from a low to high sinuosity with significant variation in flow direction. This initiated deposition of the Sarnoo to the Nosar sandstones and rejuvenated in its own system increasing the renewed localized tectonic activity (Beaumont *et al.* 2018). The contour maps of the concerned part of the hill area display the elevated patches separately with gentle slope area (Supplementary figure S6).

The cross-section A–B marks the run-off induced channels within ∼6.5 km. This analysis incorporates the delineation of five watersheds with channels flowing in different directions (figure 16B). The study discloses the channel pattern (figure 16B1) where channel 1 is sinuous, channel 2 is straight, channel 3 again sinuous, and channel 4 is straight. Section (a) in channel 2 is a straight (narrow 'V' shape valley) and prone to deep incision. Whereas, section (b) in channel 3 is wide 'V' with sinuous channel. This SW part of the Sarnoo hills bears

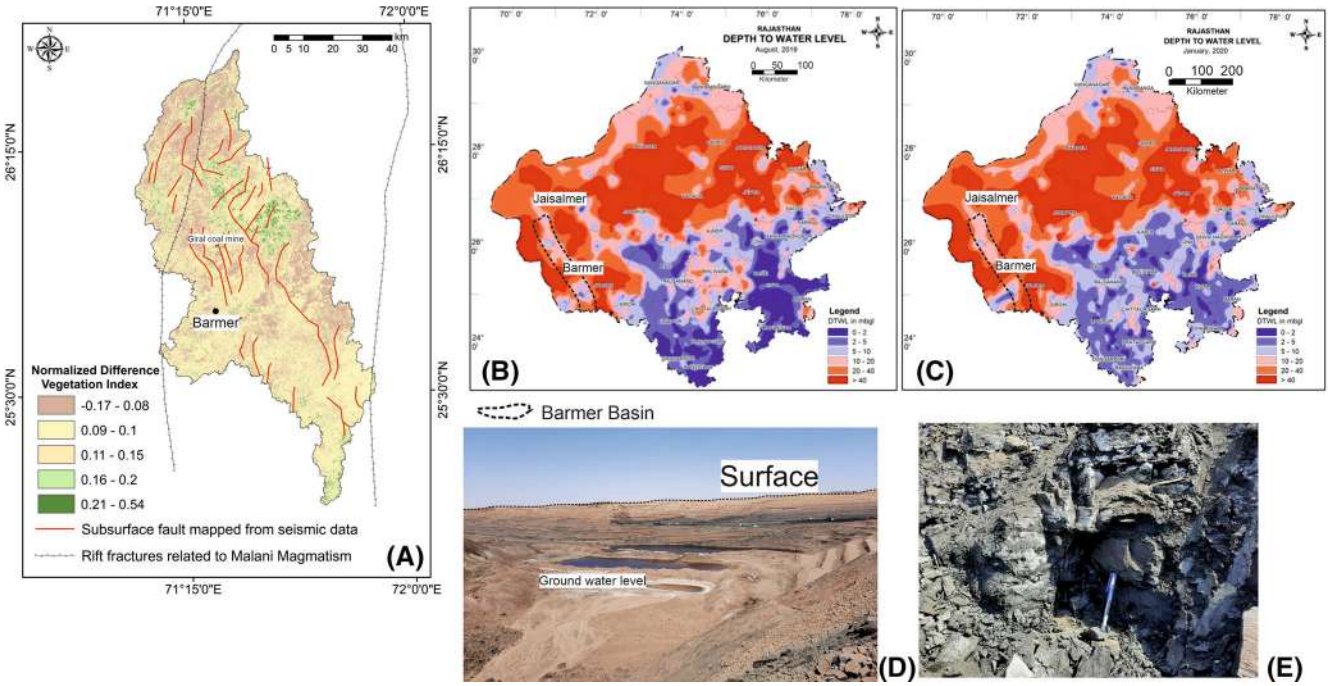

Figure 20. **(A)** Normalized difference vegetation index (NDVI) map of tectonically active watershed-1 where sub-surface faults and rift fractures have been overlaid. **(B)** Depth of water level of August 2019 in mbgl (deep tube well water level, based on report of CGWB, 2019–2020, Rajasthan) of Rajasthan where Barmer basin is marked in black. **(C)** Depth of water level of January 2020 in mbgl (deep tube well water level) of Rajasthan where Barmer basin has marked in black. **(D)** Image of Giral coal mines where groundwater level is visible in the deepest point from the surface. Extracted and delineated (from Cartosat 1) five watersheds of Barmer basin and its adjacent area.

significant evidence of geomorphic evolution under arid cycles of dynamic equilibrium with isolated inselbergs as remnants (figure 16C).

5.2.6 *Sarnoo II (25°41′19.48″N/71°47′20.90″E)*

A tectonic lake is documented (∼150 m long, 65.62 wide, 362 m perimeter). The lake is spaced in an elongated shape within the elevated hilly patch (figure 17A). Two times uplift/erosion happened (cycles C1 and C2). The first cycle produced T1 terrace, and a tectonic uplift of 4.39 m during C2 generated a T2 terrace. Several gullies and streamlets have originated from the terrace sections and flow towards the lake following the slope (figure 17B, B1, B2).

5.2.7 *Sarnoo III (25°40′11.07″N/71°46′25.54″E)*

The exposed layers of the Cretaceous Ghaggar–Hakra Formation in the eastern margin of the Barmer rift basin prominently indicate rift-margin geometries of pre-Paleogene normal faulting. The NW–SE cross-section in figure 18(A) displays the exposed extended part of the Sarnoo hill of 130.8 m in the upper elevated left bank of the old channel. The valley is ∼50 m wide, 2 m elevated, and ∼87° sloping scarp on the right bank. Towards downstream, steep cutting scarps (∼87–90°) are exposed continuously (figure 18B).

There are two points marked in red and green in figure 18(C) as 1 and 2 with distinct gorges. In section 1 in the upstream portion, the valley is 'I' shaped in section (a) followed by a wide 'V' in section (b) at downstream. The valley again becomes 'I'-shaped as a gorge towards the downstream due to steep vertical incisions than lateral erosion (figure 18C). It is a convex fifth-order surface formed by pebble-grade quartz clasts of grain. It is an area of floodplain deposition, eroded by the channel (Kraus and Hasiotis 2006). It is composed of compact conglomeratic clasts overlain by fine-grained weathered unsorted sediments. Between these, a thin iron leached layer exists. Conglomeratic clast supported depositions crop out in the scarp (Supplementary figure S7). Clast-supported conglomerates typically occur as boarder along the channels transported under high-energy (Froude *et al.* 2017) and stream power conditions. The red

box is presented under two broad layers with six layers from (a) to (f) (Supplementary figure S7). The uppermost layer 'a' is entirely weathered and flaggy, which is followed by 'b' as less flaggy, 'c' salt leached, 'd' compact with iron content, 'e' poorly-shorted rounded shaped quartz, and 'f' represents a compact layer of clast-supported conglomerate.

5.2.8 *Sarnoo IV (25°40′11.82″N/71°46′22.68″E):*

It denotes the southernmost range of the Sarnoo hill, extended along NNE–SSW. Exposed elevated patches (figure 19A) exist as the remnants of the erosional cycle where the three drainage lines are identified out of which two are prominent (figure 19B). Five small watersheds are generated due to running water following the local slopes. Tectonic instability of the channel rejuvenated it. Four to five gullies have joined channel-1 from west to east. Single-tier terraces are identified (figure 19C) in ∼400 m downstream from the probable source point (25°40′10.71″N/71°46′23.73″E). This indicates recent tectonic activity that enhanced the incision. There are three cross-sections from upstream to downstream that portray the uneven valley side-cutting (left bank slope ∼86° and right bank ∼15°) and unpaired terrace system that indicates the active tectonics (figure 19Ba–c).

In watershed 1, NDVI has been applied to find out the vegetation trend (figure 20A). Distinct vegetation lines have developed along north to south crossing the Giral coal mine, and few patches occur in isolation in the eastern boundary of the watershed. Field visit confirms that corn and maze are cultivated near the Giral Mine (∼ 26°3′55.33″N/71°20′10.27″E) where the piezometric level ranges from 7 to 8 mbgl [CGWB reports of 2019–2020 (figure 20B, C) of August 2019 and January 2020] (Cohen and Siter 1993; Gudmundsson 2000). The possible alignment of subsurface faults is plotted on the NDVI map, which predominantly reveals their correlation.

6. Conclusions

Barmer and the nearby sedimentary basins of the Western Indian Rift System underwent structural inversion, right from the tectonism related to India–Seychelles separation ∼64 Ma up to India–Asia collision that initiated from ∼55 Ma. Sedimentary and basement rocks of the basin eroded irregularly. Tectonic events are morphologically evident in terms of linear-scale and basin/watershed-scale analysis in secondary and primary levels.

Present-day river geometry, terraces, floodplains, drainage patterns, drainage density, stream order, and basin-scale parameters led to the calculation of IAT of the five watersheds. The field-based spot study of channels, gullies and valley anomalies indicates structural controls on geomorphology. Geologic history presumably controlled the fluvial flow directions, rejuvenation and bedload sediment character in response to the fifth-order landscape of the Ghaggar–Hakra Formation in the eastern part of the basin.

Elongated watershed-2, along the eastern boundary of the Barmer basin, is tectonically active as per the calculated IAT. This is also inferred from the tectonically active elongated seasonal lake adjacent to Ghaggar–Hakra outcrop hill near Sarnoo.

The hill patches of the Sarnoo area generated small-scale watersheds and channels. To the east, near the Luni channel, the existence of river terraces and Gangli basalt dykes indicate the magmatic/tectonic activity in watershed-2.

Gullies were formed profusely near all the fault-guided sections around the Fatehgarh fault area, Luni channel, Sarnoo area, towards Kiradu temple, etc. Extensive weathering and fractured flaggy rocks are found mainly in the Barmer hills area, piedmont plains, rocky pediments near Jasaiwith terraces and at places the buried pediments near Gangli and Sarnoo. These features formed due to the higher intensity of runoff, steeper slope and sediment abundance.

In watershed-1, NDVI has been applied to visualize the vegetation trend pattern. Distinct vegetation lines have developed along north to south crossing the Giral coal-mine and few patches are located in isolated form in the eastern boundary of the basin. Such precise alignment of vegetation around the Giral Mine area might be fault-controlled.

Acknowledgements

This study is funded by a seed project received from Center of Excellence in Oil, Gas and Energy, IIT Bombay (grant no. RD/0120-PSUCE19-001) awarded to SM. Thanks are due

to J Shrikanth and S N Karnekarand for assisting SM in project-related paper works. MSc thesis student of SM, Ratna Choudhari, assisted in the field. Chief Editor N V Chalapathi Rao handled this article. An anonymous reviewer is thanked for detailed comments.

Author statement

All authors except MPG did fieldwork. MB and MPG did remote sensing works. MB, SM and SDG wrote and finalized the article.

References

ALOS World 3D-30m (AW3D30) 2015 The ALOS Global Digital Surface Model (AW3D30) by Japan Aerospace Exploration Agency (JAXA); https://www.eorc.jaxa.jp/ALOS/en/index.htm.

Altaf F, Meraj G and Romshoo S A 2013 Morphometric analysis to infer hydrological behaviour of Lidder Watershed, Western Himalaya, India; *Geogr. J.* **2013** 178021.

Ansan V and Mangold N 2006 New observations of WarregoValles, Mars: Evidence for precipitation, and surface runoff; *Planet. Space Sci.* **54** 219–242.

Armitage J J, Collier J S and Minshull T A 2010 The importance of rift history for volcanic margin formation; *Nature* **465** 913–917.

Armitage J J, Collier J S, Minshull T A and Henstock T J 2011 Thin oceanic crust and flood basalts: India–Seychelles breakup; *Geochem. Geophys. Geosyst.* **12** Q0AB07, https://doi.org/10.1029/2010GC003316.

Ayaz S, Biswas M and Dhali K 2018 Morphotectonic analysis of alluvial fan dynamics: Comparative study in spatio-temporal scale of Himalayan foothill, India; *Arab. J. Geosci.* **11**(**41**) 1–16.

Babu D K and Odeh A S 1994 Discussion of production logging as an integral part of horizontal-well transient-pressure test; *SPE Formation Evaluation (Soc. Petrol. Engineer.)* **93**, ISSN 0885-923X.

Beaumont H, Clarke M S, Burley D S, Taylor A M and Mohapatra P 2018 Sedimentology and the facies architecture of the Ghaggar–Hakra Formation, Barmer Basin, India: Implications for early Cretaceous deposition on the north-western Indian Plate margin; The Depositional Record, Department of Geography and Environmental Management, University of the West of England Bristol, Bristol, UK.

Beaumont H, Clarke M S, Burley S D, Taylor A, Gould T and Mohapatra P 2015 Deciphering tectonic controls on fluvial sedimentation within the Barmer Basin, India: The Lower Cretaceous Ghaggar–Hakra Formation; Search Discov. 2015:51100, http://www.searchanddiscovery.com/pdfz/documents/2015/51100beaumont/ndx_beaumont.pdf.html.

Bladon A J, Burley S D, Clarke S M and Beaumont H 2014 Geology and regional significance of the Sarnoo Hills, eastern rift margin of Barmer Basin, NW India; *Basin Res.* **27** 636–655.

Biswas M and Dhara P 2019 Correction to: Evolutionary characteristics of meander cut-off – A hydro-morphological study of the Jalangi River, West Bengal, India; *Arab. J. Geosci.* **12** 739.

Biswas M and Paul A 2021 Application of geomorphic indices to address the foreland Himalayan tectonics and landform deformation: Matiali–Chalsa–Baradighi recess, West Bengal, India; *Quat. Int.* **585** 3–14.

Bladon A J, Clarke S M and Burley S D 2015 Complex rift geometries resulting from inheritance of pre-existing structures: Insights and regional implications from the Barmer Basin rift; *J. Struct. Geol.* **71** 136–154.

Bonini M, Souriot T, Boccaletti M and Brun J P 1997 Successive orthogonal and oblique extension episodes in a rift zone: Laboratory experiments with application to the Ethiopian Rift; *Tectonics* **16** 347–362.

Brice J C 1964 Channel patterns and terraces of the Loup Rivers in Nebraska; *Geol. Surv. Prof. Paper* **422(D)** D2–D41.

Bull W B 1978 Geomorphic Tectonic Classes of the South Front of the San Gabriel Mountains; US Geological Survey Contract Report 14-08-001-G-394, Office of Earthquakes, Volcanoes and Engineering, Menlo Park.

Bull W B and McFadden L D 1977 Tectonic geomorphology north and south of the Garlock fault, California; In: *Geomorphology in arid regions* (ed.) Doehering D O, Proceedings at the Eighth Annual Geomorphology Symposium, pp. 115–138.

Chatterjee S, Goswami A and Scotese C R 2013 The longest voyage: Tectonic, magmatic, and paleoclimatic evolution of the Indian plate during its northward flight from Gondwana to Asia; *Gondwana Res.* **23** 238–267.

Chenet A L, Quidelleur X, Fluteau F, Courtillot V and Bajpai S 2007 ^{40}K–^{40}Ar dating of the Main Deccan large igneous province: Further evidence of KTB age and short duration; *Earth Planet*; *Sci. Lett.* **263** 1–15.

Cohen A J B and Siter N 1993 Influence of faults on groundwater flow and transport at Yucca Mountain, Nevada; Lawrence Berkeley National Laboratory, https://www.osti.gov/servlets/purl/926686-3Vpavg/.

Collier J S, Sansom V, Ishizuka O, Taylor R N, Minshull T A and Whitmarsh R B 2008 Age of Seychelles-India break-up; *Earth Planet. Sci. Lett.* **272** 264–277.

Compton P M 2009 The geology of the Barmer Basin, Rajasthan, India and the origins of its major oil reservoir, the Fatehgarh Formation; *Petrol. Geosci.* **15** 117–130.

Conybeare C E B 1976 *Geomorphology of oil and gas fields in sandstone bodies; Developments in Petroleum Science 4*, Elsevier, Amsterdam, 296p.

Cox R T 1994 Analysis of drainage-basin symmetry as a rapid technique to identify areas of possible quaternary tilt-block tectonics: An example from the Mississippi Embayment; *Geol. Soc. Am. Bull.* **106** 571–581.

Czerniawska J and Chlachula J 2017 Report, field trip in the Thar Desert; *Landform Anal.* **35** 21–26.

Dasgupta S K 1975 A revision of the Mesozoic–Tertiary stratigraphy of the Jaisalmer Basin, Rajasthan; *Indian J. Earth Sci.* **2** 77–94.

Dasgupta S K, Dhar C L and Singh N P 1975 A note on the occurrence of a bioclastic foraminiferal bed on the top offuller's earth sequence in Barmer District, Rajasthan; *Sci. Culture* **41** 127–129.

Dasgupta S and Mukherjee S 2017 Brittle shear tectonics in a narrow continental rift: Asymmetric nonvolcanic Barmer Basin (Rajasthan, India); *J. Geol.* **125** 561–591.

Dasgupta S and Mukherjee S 2019 Remote sensing in lineament identification: Examples from western India; In: *Problems and solutions in structural geology and tectonics. Developments in Structural Geology and Tectonics Book Series* (ed.) Mukherjee S, **5**, 205–221, Elsevier, ISSN: 2542-9000, ISBN: 9780128140482.

Dasgupta S, Biswas M, Mukherjee S and Chatterjee R 2022 Structural evolution and sediment depositional system along the transform margin–Palar–Pennar basin, Indian east coast; *J. Petrol. Sci. Engineer.* **211** 110155.

Dehbozorgi M, Pourkermani M, Arian M, Matkan A A, Motamedi H and Hosseiniasl A 2010 Quantitative analysis of relative tectonic activity in the Sarvestan area, central Zagros, Iran; *Geomorphology* **121** 329–341.

Dhanya V 2014 Basin asymmetry and associated tectonics: A case study of Achankovil river basin, Kerala; *Trans. Inst. Indian Geograph.* **36(2)** 207–215.

Dolson J, Burley S D, Sunder V R, Kothari V, Naidu B, Whiteley N P, Farrimond P, Taylor A, Direen N and Ananthakrishnan B 2015 The discovery of the Barmer Basin, Rajasthan, India and its petroleum geology; *AAPG Bull.* **125** 351–371.

EarthExplorer (EE) United States Geological Survey (USGS), https://earthexplorer.usgs.gov/.

Froude M J, Alexander J, Barclay J and Cole P 2017 Interpreting flash flood palaeoflow parameters from antidunes and gravel lenses: An example from Montserrat, West Indies; *Sedimentology* **64** 1817–1845.

Gudmundsson A 2000 Active fault zones and groundwater flow; *Geophys. Res. Lett.* **27** 2993–2996.

Hack J 1957 Studies of longitudinal stream profiles in Virginia and Maryland; *Geol. Surv. Prof. Paper* **294(B)** 45–95.

Haggett P and Chorley R J 1969 Network Analysis in Geography; Edward Arnold, London.

Hamdouni R El, Irigaray C, Fernández T, Chacón J and Keller E A 2008 Assessment of relative active tectonics, southwest border of the Sierra Nevada (southern Spain); *Geomorphology* **96(1–2)** 150–173, https://doi.org/10.1016/j.geomorph.2007.08.004.

Hare P W and Gardner T W 1985 Geomorphic Indicators of Vertical Neotectonism along Converging Plate Margins, Nicoya Peninsula, Costa Rica; In: *Tectonic Geomorphology* (eds) Morisawa M and Hack J T, Proceedings of the 15th Annual Binghamton Geomorphology Symposium, Allen and Unwin, Boston, pp. 123–134.

Horacio J 2014 River sinuosity index: Geomorphological characterization; CIREF and Wetlands International European Association, 8p.

Horton R E 1945 Erosional development of streams and their drainage basins: Hydrophysical approach to quantitative morphology; *Bull. Geol. Soc. Am.* **56** 275–370.

Howard A D 1967 Drainage analysis in geologic interpretation: a summation; *AAPG Bull.* **51** 2246–2259.

India Districts ADM2 GADM from ArcGIS Hub; https://hub.arcgis.com/datasets/2b37b84e67374fb98577c20ef8be6c62_0.

Kale V S, Sengupta S, Achyuthan H and Jaiswal K M 2014 Tectonic controls upon Kaveri River drainage, cratonic Peninsular India: Inferences from longitudinal profiles, morphotectonic indices, hanging valleys and fluvial records; *Geomorphology* **227** 153–165.

Kar A 1987 Origin and transformation of longitudinal sand dunes in the Indian Desert; *Zeitschrift fur Geomorphol.* **31** 311–337.

Kar A 1990 Themegabarchanoids of the Thar: Their environment, morphology and relationship with longitudinal dunes; *Geograph. J.* **156** 51–61.

Kar A 2011 Quaternary Geomorphic Processes and Landform Development in the Thar Desert of Rajasthan; In: *Landforms processes and environment management*, pp. 223–254, ISBN 81-87500-58-1.

Keller E A and Pinter N 2002 *Active tectonics: Earthquakes, uplift, and landscape;* (2nd edn), Englewood Cliffs, New Jersey, Prentice Hall, 362p.

Kraus M and Hasiotis S 2006 Significance of Different Modes of Rhizolith preservation to interpreting paleoenvironmental and paleohydrologic settings: Examples from Paleogene Paleosols, Bighorn Basin, Wyoming, U.S.A; *J. Sedim. Res.* **76** 633–646, https://doi.org/10.2110/jsr.2006.052.

Lavarini C, Júnior M P A, Oliveira S F and Carvalho A 2016 neotectonics, river capture and landscape evolution in the highlands of SE Brazil; *Mercator, Fortaleza* **15** 95–119.

Lee C and Tsai L L 2009 A quantitative analysis for geomorphic indices of longitudinal river profile: A case study of the Choushui River, Central Taiwan; *Environ. Earth Sci.* **59** 1549–1558.

Mahmood S and Gloaguen R 2012 Appraisal of active tectonics in Hindu Kush: Insights from DEM derived geomorphic indices and drainage analysis; *Geosci. Front.* **3** 407–428.

Mazumder S, Dave H D, Samal J K and Mitra D S 2012 Delieation of basement related fault closures in eastern part of Purnea basin based on morphometric analysis; *AAPG Bull.* **8** 41–48.

Moharana P C, Gaur M K, Choudhary C, Chauhan J S and Rajpurohit R S 2013 A system of Geomorphological Mapping for Western Rajasthan with Relevance for Agricultural Land Use; *Ann. Arid Zone* **52** 163–180.

Morisawa M 1985 *Rivers – Forms and Process;* 1st edn, State University of New York at Binghamton.

Mueller J E 1968 An Introduction to the Hydraulic and Topographic Sinuosity Indexes 1. *Ann. Assoc. Amer. Geogr.* **58** 371–385, https://doi.org/10.1111/j.1467-8306.1968.tb00650.x.

Ozyavuz M, Bilgili B C and Salici A 2015 Determination of vegetation changes with NDVI method; *J. Environ. Protect. Ecol.* **16(1)** 264–273.

Pandit M K, Shekhawat L S, Ferreira V P, Sial A N and Bohra S K 1999 Trondhjemite and granodiorite assemblage from west of Barmer: Probable basement from Malani magmatism in western India; *J. Geol. Soc. India* **53** 89–96.

Pareta K and Pareta U 2011 Quantitative morphometric analysis of a watershed of Yamuna Basin, India using ASTER (DEM) data and GIS; *Int. J. Geomat. Geosci.* **2** 248–269.

Paul A and Biswas M 2019 Changes in river bed terrain and its impact on flood propagation – a case study of River Jayanti, West Bengal, India; *Geom. Nat. Hazards Risk* **10** 1928–1947, https://doi.org/10.1080/19475705.2019.1650124.

Prakash K, Mohanty T and Pati J K *et al.* 2017 Morphotectonics of the Jamini River basin, Bundelkhand Craton,

Central India using remote sensing and GIS technique; *Appl. Water Sci.* **7** 3767–3773.

Roy A B and Jokhar S R 2002 *Geology of Rajasthan (Northwest India): Precambrian to recent;* Scientific Publishers, Jodphur, India.

Sarah A, Drummonda A H and Erkelingb G 2014 Drainage Pattern; *Encyclopaedia of Planetary Landforms*, https://doi.org/10.1007/978-1-4614-9213-9_119-1.

Schumm S A and Khan H R 1972 Experimental study of channel patterns; *Geol. Soc. Am. Bull.* **83**(**1**) 755–1770.

Schumm S A 1956 The evolution of drainage systems and slopes in bad lands at Perth, Amboi, New Jersey; *Geol. Soc. Am. Bull.* **67** 597–646.

Sen A, Pande K, Hegner E, Sharma K K, Dayal A M, Sheth H C and Mistry H 2012 Deccan volcanism in Rajasthan: ^{40}Ar–^{39}AR geochronology and geochemistry of the Tavidar volcanic suite; *J. Asian Earth Sci.* **59** 127–140.

Sharma G, Champati R P K and Mohanty S 2018 Morphotectonic analysis and GNSS observations for assessment of relative tectonic activity in Alaknanda basin of Garhwal Himalaya, India; *Geomorphology* **301** 108–120.

Sharma K K 2005 Malani magmatism: An extensional lithospheric tectonic origin; *Geol Soc. Am. Spec. Paper* **388** 463–476.

Singh C K 2015 Middle Ganga plain; may be on the verge of seismic shock; *J. Geol. Soc. India* **85** 511–513.

Singh S 1977 *Geomorphological Investigation of the Rajasthan Desert*; Central Arid zone Research Institute, Jodhpur, Monograph no. 7, pp. 10-62.

Singh S, Pandey S and Ghose B 1971 Geomorphology of the middle Lllni basin of western Rajasthan, India; *Ann. Arid Zone* **10** 1–14.

Singh D S, Prajapati S K, Singh P, Singh K and Kumar D 2015 Climatically induced levee break and flood risk management of the Gorakhpur region, Rapti River Basin, Ganga Plain, India; *J. Geol. Soc. India* **85** 79–86.

Sisodia M S and Singh U K 2000 Depositional environment and hydrocarbon prospects of the Barmer Basin, Rajasthan, India; *Nafta Zagreb (croatia)* **51** 309–326.

Storey M, Mahoney J J, Saunders A D, Duncan R A, Kelley S P and Coffin M F 1995 Timing of hot-spot related volcanism and the break-up, Madagascar, and India; *Science* **267** 852–855.

Strahler A N 1952 Hypsometric (area-altitude) analysis of erosional topography; *Geol. Soc. Am. Bull.* **63** 1117–1142.

Torsvik T H, Pandit M K, Redfield T R, Ashwal L D and Webb S J 2005 Remagnetization of Mesozoic limestones from the Jaisalmer basin, NW India; *Geophys. J. Int.* **161** 57–64.

Twidale C R 2004 River patterns and their meaning; *Earth Sci. Rev.* **67** 159–218.

Whipple K, Wobus C, Crosby B, Kirby E and Sheenan D 2007 New tools for quantitative geomorphology: Extracting and interpretation of stream profiles from digital topographic data;*GSA Annual Meeting*, Boulder, USA.

Wobus C, Whipple K, Kirby E, Snyder N, Johnson J, Spyropoulou K, Crosby B and Sheehan D 2006 Tectonics from topography: Procedures, promise, and pitfalls; In: Tectonics, climate, and landscape evolution; *Geol. Soc. Am. Spec. Paper* **398** 55–74.

Wołosiewicz B 2018 The influence of the deep seated geological structures on the landscape morphology of the Dunajec River catchment area, Central Carpathians, Poland and Slovakia. Contemperory trends; *Geosci.* **72** 1–47.

Zävoianu I 1985 Hypsometric curves and longitudinal stream profiles; *Dev. Water Sci.* **20** 185–200.

Zernitz E R 1932 Drainage patterns and their significance; *J. Geol.* **40** 498–521.

Ziyad E 2014 Relationship between tectonic activity, fluvial system and river morphology in the Dohuk catchment, Iraqi Kurdistan; *Géomorphol Relief, Processes, Environ.* **20** 91–100.

Corresponding editor: N V Chalapathi Rao